RESEARCH ARTICLE

Characterization of adenine phosphoribosyltransferase (APRT) activity in *Trypanosoma brucei brucei*: Only one of the two isoforms is kinetically active

Kayla Glockzin[ID]**, Thomas D. Meek**[ID]***, Ardala Katzfuss**[ID]*****

Department of Biochemistry and Biophysics, Texas A&M University, College Station, Texas, United States of America

* Thomas.Meek@ag.tamu.edu (TDM); ardalakatzfuss@gmail.com (AK)

Abstract

Human African Trypanosomiasis (HAT), also known as sleeping sickness, is a Neglected Tropical Disease endemic to 36 African countries, with approximately 70 million people currently at risk for infection. Current therapeutics are suboptimal due to toxicity, adverse side effects, and emerging resistance. Thus, both effective and affordable treatments are urgently needed. The causative agent of HAT is the protozoan *Trypanosoma brucei* ssp. Annotation of its genome confirms previous observations that *T. brucei* is a purine auxotroph. Incapable of *de novo* purine synthesis, these protozoan parasites rely on purine phosphoribosyltransferases to salvage purines from their hosts for the synthesis of purine monophosphates. Complete and accurate genome annotations in combination with the identification and characterization of the catalytic activity of purine salvage enzymes enables the development of target-specific therapies in addition to providing a deeper understanding of purine metabolism in *T. brucei*. In trypanosomes, purine phosphoribosyltransferases represent promising drug targets due to their essential and central role in purine salvage. Enzymes involved in adenine and adenosine salvage, such as adenine phosphoribosyltransferases (APRTs, EC 2.4.2.7), are of particular interest for their potential role in the activation of adenine and adenosine-based pro-drugs. Analysis of the *T. brucei* genome shows two putative *aprt* genes: APRT1 (Tb927.7.1780) and APRT2 (Tb927.7.1790). Here we report studies of the catalytic activity of each putative APRT, revealing that of the two *T. brucei* putative APRTs, only APRT1 is kinetically active, thereby signifying a genomic misannotation of Tb927.7.1790 (putative APRT2). Reliable genome annotation is necessary to establish potential drug targets and identify enzymes involved in adenine and adenosine-based pro-drug activation.

Author summary

Neglected Tropical Diseases, including Human African Trypanosomiasis (HAT), are defined by the World Health Organization as a diverse group of 20 different diseases that disproportionally affect the world's poorest populations. HAT is endemic to 36 African

countries and approximately 70 million people worldwide are currently at risk for infection. Current therapeutics are suboptimal due to toxicity, adverse side effects, and emerging resistance. The causative agent of HAT is *Trypanosoma brucei* ssp. Unlike humans, these protozoan parasites rely on purine phosphoribosyltransferases to salvage purine bases from their hosts for the synthesis of DNA and RNA. Here we report on the characterization of adenine phosphoribosyltransferase (APRT) activity in *Trypanosoma brucei brucei*. Enzymes involved in adenine and adenosine salvage, such as APRTs, are of particular interest for their potential role in the activation of adenine and adenosine-based pro-drugs. Our studies reveal that of the two putative APRTs, only APRT1 is kinetically active under physiological conditions. Accurate genome annotations in combination with the characterization of purine salvage enzymes allows the development of target-specific therapies.

Introduction

Trypanosoma brucei ssp. is the etiological agent of Human African Trypanosomiasis (HAT), also known as sleeping sickness. *Trypanosoma brucei gambiense* and *Trypanosoma brucei rhodesiense* cause, respectively, chronic and acute forms of this disease in humans [1,2], for which the chronic infection is more prevalent (> 90% of reported cases) [3]. HAT presents initial symptoms of headache, fever, and fatigue; and is mainly transmitted horizontally by the vector tsetse flies of the genus *Glossina* [4], but also vertically from mother to offspring [5], with evidence of sexual transmission [6]. Once in the central nervous system (CNS), the parasites alter sleeping habits, cause mood swings, impairment of reasoning and mental processing, followed by coma and death if untreated [7–9]. Progression of HAT leads to demyelination in the CNS, making it impossible to cure even after clearance of parasites [1]. HAT is endemic to 36 African countries; threatening an estimated 70 million people [3,10].

No vaccine or prophylactic therapy is available [8], and the current standard of treatment is poor. Five drugs are currently used to treat HAT. Pentamidine and Suramin are used in early stages of the infection. Melarsoprol is the first-line treatment for late-stage disease; and Eflornithine is effective only against *T. brucei gambiense* infections, but the dosage necessary limits its use. Treatment failure due to patient non-compliance ranges around 30%, with high rates of death related to toxicity of Melarsoprol (up to 12%) [1,3]. The World Health Organization (WHO) has emphasized the need for intensive efforts to treat HAT, including the development of novel therapies [11]; nonetheless, until recently the last drug introduced for treatment was Eflornithine in 1990 [3]. In 2019, the WHO added fexinidazole - a nitroimizadole that inhibits DNA synthesis, to its *T. brucei gambiense* HAT treatment guidelines as a first line treatment [12,13], followed by the European Medicines Agency (EMA) [14] and U.S. Food and Drug Administration (FDA) [15] approvals in 2018 and 2021, respectively. Fexinidazole showed >90% success rate and has been approved for use in patients older than 6 years old and weighing at least 20 Kg for treatment of early and late-stage HAT as an oral drug administered once a day for 10 days [12]. Reported side-effects are considered mild (headache, vomiting, insomnia, nausea, asthenia, tremor, and decreased appetite) [16], but inpatient treatment is deemed mandatory in cases of history of psychiatric disorders, children under 35 Kg, and cases with elevated white blood cells (> 100/µL) [12]. Pharmacokinetics studies indicate the presence of fexinidazole in breastmilk, and its effects and benefits during pregnancy are still under investigation [12].

Difficulties in the development of novel drugs for the treatment of Neglected Tropical Diseases include many social, economic, and political factors. In the case of HAT, these

complications are exacerbated by the intrinsic complexities of the *T. brucei* ssp. convoluted life cycle. *T. brucei* ssp. is a single-cell obligate parasite with human and insect hosts. To complete its life cycle, the parasite must adapt to the widely different environments it faces in both hosts, and it accomplishes this task by modulating its gene expression, metabolic state, morphology, and reproduction strategies [4,17–19]. Inside the tsetse fly, procyclic forms of trypanosomes adapt to a range of microenvironments including the proventriculus, salivary glands, anterior midgut and posterior midgut [20–22]. In the human host, the bloodstream forms of *T. brucei* ssp. infect blood and interstitial fluids, including cerebrospinal fluid and lymph [23].

The genome sequencing of *T. brucei* was completed in 2005 for the *T. brucei brucei* strain TREU927. *T. brucei brucei* causes disease (Nagana) in cattle and other vertebrates [24], however it is incapable of infecting humans and is considered the model organism for the infectious subspecies [25–27]. The data derived from the genomic annotation, allied to several proteomics studies that identified the differentially expressed genes along *T. brucei*'s life cycle [28–31] allows the use of target-specific strategies of drug development as a promising way to identify and develop novel therapies [32]. Genomic annotation of *T. brucei brucei* corroborate previous observations that, as other parasitic protozoa, *T. brucei* ssp. is a purine auxotroph [32,33], being incapable of synthesizing purine nucleotides *de novo*, and relying on uptake from the hosts to afford its metabolic needs via the purine salvage pathway. Trypanosomes incorporate purine nucleobases and purine analogs by a highly selective nucleobase/proton symporter system with differential expression during procyclic and bloodstream stages [34–37]. Once inside the cell, the purine nucleobases and nucleosides are further converted into nucleotides by enzymes of the salvage pathway, including three purine phosphoribosyltransferases which have some overlapping substrate specificity. Many of the enzymes of purine salvage present stage-specific expression profiles [38]; and previous cellular studies indicate that any single purine can be sufficient to support *T. brucei* growth *in vitro* [39]. Proper genome annotation, and the identification and characterization of the catalytic activity of purine salvage enzymes are key steps not only for understanding *T. brucei* metabolic pathways, but to aid the development of target-specific novel therapies. The enzymes involved in adenine and adenosine salvage are of particular interest for their potential role in the activation of adenine and adenosine-based antimetabolite pro-drugs [40–43].

In this work, we describe the kinetic characterization of *T. brucei brucei* adenine phosphoribosyltransferase (APRT) activity. APRTs (EC 2.4.2.7) are enzymes of the purine salvage pathway, catalyzing the formation of adenosine monophosphate (AMP) from 5-phospho-α-D-ribose-1-diphosphate (PRPP) and adenine (Fig 1). There are two putative *aprt* genes predicted into *T. brucei brucei* genome. APRT1 and APRT2 are in tandem on chromosome 7 and have low amino-acid sequence identity (22%). Furthermore, APRT1 has been shown to be a cytosolic protein, while APRT2 co-localizes to the glycosome [31]. APRT1 was also demonstrated to be expressed on both bloodstream forms and procyclic trypanosomes, while APRT2 expression
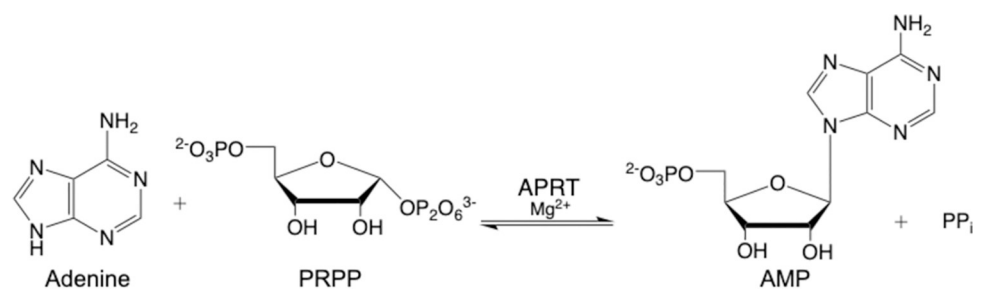

Fig 1. Reaction catalyzed by adenine phosphoribosyltransferase (APRT, EC 2.4.2.7).

was mainly detected on procyclic forms [40]. A previous phenotypic study of APRT activity in *T. brucei* was conducted with an APRT1/APRT2 double knockout [40]. Other reports on APRT were performed using total cell extract activity [44], detection of mRNA [29], co-immunoprecipitation [45], or proteomic analyses [31]. The APRTs have been evaluated as potential drug targets, however previous work has been unsuccessful in evaluating APRT1 and APRT2 independently [46]. In this study, we focus on the catalytic activity of each putative APRT individually. Our results reveal that of the two *T. brucei brucei* genes annotated as putative APRTs, only one, APRT1, is biologically relevant for catalyzing the conversion of adenine into AMP.

Methods

Protein cloning, expression, and purification

APRT1 (Tb927.7.1780, UNIPROT access code Q57V32) and APRT2 (Tb927.7.1790, UNIPROT access code Q57V31) were codon optimized for expression in *Pichia pastoris*. Overhangs were added to the 5' and 3' ends of each ORF for assembly into the pPICZ vectors (S1 Appendix). Each gene was initially cloned into pET-28a(+) vectors, using *Nde*I and *Hind*III restriction sites (Genscript, USA). The plasmids pET-28a(+)::*aprt1-Ntag*, pET-28a(+):: *aprt1-Ctag*, pET-28a(+)::*aprt2-Ntag* and pET-28a(+)::*aprt2-Ctag* were linearized by PCR (S2 Appendix) and cloned into the pPICZ vectors (pPICZ-Ntag and pPICZ-Ctag) using a HiFi DNA assembly kit (NEB). Assembled products were subsequently transformed into NEB 5-alpha competent *Escherichia coli* cells using heat-shock and incubated overnight at 37°C on LB agar plates containing kanamycin 50 μg mL^{-1}. Plasmids were linearized by PCR prior to transformation into *P. pastoris* strain smPP, using primers forward (5' to 3') GCTGTCTTGG AACCTAATATG, and reverse (5' to 3') TGTCAGTTTTGGGCCATTTG. The pPICZ-Ctag vector contains a cleavage site for the Tobacco Etch Virus (TEV) protease upstream of a C-terminal mCherry tag followed by a Strep-II tag and 6×His-tag. The pPICZ-Ntag vector contains an N-terminal TEV protease cleavage site downstream from a 6×His-tag followed by a mCherry tag (S1 and S2 Figs). The clones with the highest expression levels of APRT1 and APRT2 were selected based on mCherry expression levels (S3 Fig). One single colony was used to inoculate 25 mL of Yeast extract-Peptone-Dextrose (YPD) media in the presence of zeocin 50 μg mL^{-1}. Pre-starting cultures were incubated overnight at 30°C in an orbital shaker set at 200 RPM. A 10 mL sample of pre-starting culture was used to inoculate 600 mL of Buffered Glycerol Complex Media (BMGY) in the presence of zeocin 50 μg mL^{-1}. Starter cultures were grown at 30°C and 200 RPM for 24 hours and harvested by centrifugation 2,000 × *g*, 5 min, at room temperature (RT). Pellets were resuspended with 40 mL of fresh Buffered Methanol Complex Media (BMMY). 10 mL samples of the resuspended pellet were used to inoculate 600 mL of BMMY media in the presence of zeocin 50 μg mL^{-1}. Cultures were grown at 30°C and set at 200 RPM for 24 hours. Protein expression was induced by addition of methanol at a final concentration of 0.5% (v/v). Cells were further grown under these conditions for 24 hours. Cells were harvested by centrifugation at 2,000 × *g*, washed with 50 mM EPPS (pH 8.3) and stored at -80°C until purification. 10 grams of cell paste were resuspended in 50 mM Na$_2$HPO$_4$/ NaH$_2$PO$_4$ (pH 7.4), 300 mM NaCl (Resuspension Buffer) and lysed by microfluidizer (4 cycles at 30 kpsi). Lysed cells were centrifuged at 18,000 RPM and the supernatant fraction containing the soluble protein(s) of interest (POI) were taken for purification. The His-tagged proteins were purified using HisPur Ni-NTA resin (Thermo Fisher Scientific), at RT. Protein binding to the column was carried out in Resuspension Buffer containing 20 mM imidazole. The bound protein(s) was washed with increasing concentrations of imidazole (20–50 mM) in Resuspension Buffer and eluted in 10 column volumes (CV) of this buffer containing a gradient of 300– 600 mM imidazole. Fractions containing the POI, as inferred by analysis with 12% SDS-PAGE

stained with Coomassie Blue, were pooled and dialyzed against 50 mM EPPS (pH 8.0), 300 mM NaCl. Tagged proteins were processed with TEV protease to remove the respective N or C-terminal tags according to the methodology described in [47]. The cleaved protein mixture was subjected to a second round of purification by chromatography on Ni-NTA resin following the same gradient for elution. Flow through fractions containing tag-less APRT1 or APRT2, as inferred by 12% SDS-PAGE stained with Coomassie Blue, were pooled and dialyzed against 50 mM HEPES (pH 7.4), 300mM NaCl, 50 mM L-Arginine, and 50 mM L-Glutamate. Homogeneous APRT1 was stored in the presence of 10% glycerol (v/v), 2.5mM TCEP at -80˚C. Homogeneous APRT2 was stored in the presence of 10% glycerol (v/v) at -80˚C.
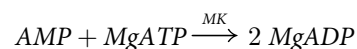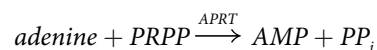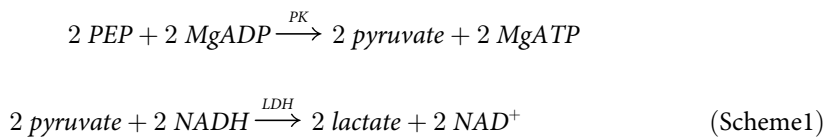
Discontinuous APRT activity assay (HPLC)

All chemicals were purchased from Sigma Aldrich, unless stated otherwise. PRPP concentrations were corrected for its purity as indicated by the supplier (75% purity). 9-deazaadenine was purchased from AA blocks (AA0037QI). Unless otherwise indicated, all kinetic assays were performed at RT.

For the forward (biosynthetic) assay of APRT, reaction mixtures contained 50 mM EPPS (pH 8.3), 12 mM $MgCl_2$ (Assay Buffer), with 1 mM PRPP, 150 μM adenine, 0.03 U inorganic pyrophosphatase (EC 3.6.1.1, Thermo Fisher Scientific) and APRT1 (0.1–25 μM) or APRT2 (0.2–25 μM). Reactions were incubated for 30 min and overnight, and were stopped by filtration to remove enzymes, using an Amicon Ultra (0.5 mL) filter with a 10,000 kDa cutoff, followed by centrifugation at 14,000 RPM for 25 min. Reverse reaction mixtures were treated similarly, and reactions mixtures containing 150 μM AMP, 1 mM inorganic pyrophosphate, and 4 μM *E. coli* K12 adenine deaminase (EC 3.5.4.2) [48], and APRT1 (0.1–25 μM) or APRT2 (0.2–25 μM). Individual chromatography standards contained 150 μM of adenine, AMP, or hypoxanthine in Assay Buffer. Negative controls were set in the same conditions as reaction mixtures, in the absence of APRT1 or APRT2. The nucleobase/nucleoside content of samples was analyzed by HPLC (high-performance liquid chromatography) using an Ultimate 3000 (Thermo Fisher Scientific) system equipped with a diode-array detector (DAD). Samples were analyzed on a Synergi Fusion-RP (4 μM, 4.6 × 150 mm) column. 15 μL of samples were injected onto the column and eluted with a gradient from 3 to 40% Solvent B over 10 minutes at flow rate of 1 mL min^{-1}. Solvent A: 20 mM ammonium acetate pH 4.5, Solvent B: 100% acetonitrile. Nucleobases and nucleotides were monitored at 260 nm.

Continuous coupled enzyme assay for APRT activity

Steady-state kinetic assays for the forward reaction were measured using a coupled enzyme system composed of myokinase (MK), pyruvate kinase (PK), and lactate dehydrogenase (LDH) to catalyze the conversion of the AMP product to, respectively, ADP, pyruvate, lactate and NAD$^+$; formation of the latter was monitored spectrophotometrically at 340nm (Scheme 1). The assays were carried out following the method described in [49] with some modifications. All assays were carried out in 100 mM HEPES buffer (pH 7.8) in the presence of 25 mM $MgCl_2$, 1 mM ATP, 0.5 mM PEP, 300 μM NADH, 36 U mL^{-1} MK, 50 U mL^{-1} PK, and 36 U mL^{-1} LDH in a total volume of 250 μL. The conversion of NADH into NAD$^+$ was monitored at 340 nm ($\varepsilon = 6220$ M^{-1} cm^{-1}).

$$adenine + PRPP \xrightarrow{APRT} AMP + PP_i$$

$$AMP + MgATP \xrightarrow{MK} 2\ MgADP$$

$$2\ PEP + 2\ MgADP \xrightarrow{PK} 2\ pyruvate + 2\ MgATP$$

$$2\ pyruvate + 2\ NADH \xrightarrow{LDH} 2\ lactate + 2\ NAD^+ \qquad \text{(Scheme1)}$$

Apparent kinetic parameters for APRT1 and APRT2 (app K_M, app k_{cat}, and app k_{cat}/K_M) were determined for adenine from initial velocity measurements in duplicate or triplicate with at least seven varied substrate concentrations, and at apparent saturating concentrations of PRPP (1 mM). Reaction mixtures of 250 µL contained adenine 2.5–60 µM in the presence of apparent saturating concentrations of PRPP (1 mM). Kinetic parameters were calculated by fitting of initial rate data to Eq (1) using GraphPad Prism 9.2 software [50]. Initial velocity data (K_M, k_{cat}, and k_{cat}/K_M) for recombinant APRT1 (200 nM) were determined as plots of changing-fixed concentration of adenine (1–20 µM) *vs*. variable PRPP (10–250 µM), or as changing-fixed concentrations of PRPP (25–150 µM) *vs*. variable adenine (1.5–50 µM), and data were fitted to Eq (2).

Initial velocity data using mixtures of APRT1 and APRT2

Purified APRT1 (2.5 µM) and APRT2 (2.5 µM) were incubated in a 1:1 equimolar ratio on ice for 4 hours. 5 µM APRT1 was diluted in half to serve as a dilution control. Kinetic assays were performed as described above for the continuous APRT activity assay. 200 nM of APRT (APRT1 or the APRT1:APRT2 mixture) was added to the assay mixture to start the reaction. The dilution control containing only APRT1 at 100 nM was included for comparison to the APRT1:APRT2 mixture. Assays were performed in triplicate.

Inhibition studies

To determine if the inhibition pattern of 9-deazaadenine against adenine and PRPP was competitive, uncompetitive, or noncompetitive, initial velocity data were collected in the presence of five apparent non-saturating concentrations of 9-deazaadenine. An inhibition pattern of 9-deazaadenine *vs*. adenine was ascertained by initial velocity data plotted as double-reciprocal plots of changing-fixed concentration of 9-deazaadenine (0–300 µM) *vs*. variable adenine (2.5–150 µM) at apparent saturating conditions of PRPP (1 mM). The 9-deazaadenine inhibition pattern against PRPP was determined as double reciprocal plots of initial velocity data in the presence of changing-fixed concentrations of 9-deazaadenine (0–600 µM) *vs*. variable PRPP (12.5–1000 µM) at apparent saturating concentration of adenine (100 µM). Inhibition data were fitted to Eqs (3)–(5). AMP formation was measured as previously described with the continuous coupled enzyme APRT activity assay.

Crosslinking assays

Homogeneous APRT1, APRT2-Ntag, and APRT2-Ctag were treated with dimethyl suberimidate (DMS) according to the method of Davies and Stark [51], in order to assess the extent to which homodimers or other multimeric forms existed in solution, as exemplified by protein cross-linking. Briefly, reaction mixtures containing 0.2 M triethanolamine (pH 8.5) and purified APRT (17.8, 35, 69, or 140 µg mL^{-1}) in the presence or absence of 8.7 mM DMS were incubated at RT for 5–8 hours, then denatured with SDS-PAGE sample loading buffer. The samples were subjected to analysis by 12% SDS-PAGE stained with Coomassie Blue to ascertain the respective levels of monomeric and multimeric forms of the enzymes that were present.

Size exclusion chromatography (SEC) of homogenous APRT1 and APRT2

To verify the oligomeric state and to ensure purified protein is not aggregated, APRT1 and APRT2 were subjected to SEC. Purified APRT1 and APRT2 were concentrated to 13.8 mg mL^{-1} and 10.8 mg mL^{-1} respectively. 200 μL of concentrated APRT1 or APRT2 were applied to a GE Superdex 200 Increase 10/300 GL SEC column using an ÄKTA pure (GE Healthcare). Proteins were eluted off with 1.2 CV of SEC Buffer: 50 mM HEPES (pH 7.8), 300 mM NaCl, 50 mM L-arginine, 50 mM L-glutamate. Prior to sample application the column was calibrated with lyophilized standards ranging from 1,350 to 670,000 Da molecular weight, containing a mixture of thyroglobulin, bovine γ-globulin, chicken ovalbumin, equine myoglobin, and vitamin B12 (BioRad, Cat #1511901) resuspended in SEC Buffer. Samples were compared to the standard to ascertain the M$_r$ (relative molecular weight), which is indicative of the oligomeric state.

Evaluation of other nucleobase substrates of APRT2

APRT2 enzyme activity was tested spectrophotometrically using alternative N-containing nucleophiles as possible substrates, including orotate, uracil, hypoxanthine, guanine, and xanthine. All assays were conducted in assay buffer containing 1 mM PRPP, APRT2 (25–50 μM), and 150 μM of nucleobase, in a final volume of 250 μL. Possible activities were assayed as follows: orotate phosphoribosyltransferase (OPRT–EC 2.4.2.10) activity was measured as described in [52], where formation of OMP was monitored at 293 nm. Hypoxanthine-guanine-xanthine phosphoribosyltransferase (HGXPRT–EC 2.4.2.8) activity was measured as described in [53,54]. Formation of IMP, GMP, and XMP were monitored at, respectively, 245 nm, 257.5 nm, and 255 nm. Uracil phosphoribosyltransferase (UPRT–EC 2.4.2.9) activity was measured as described in [55], in which monitoring of UMP formation was conducted at 280 nm. The ability of APRT2 to catalyze the synthesis of PRPP from ATP and ribose-5-phosphate (PRPP synthetase—EC 2.7.6.1) was evaluated using the described coupled-enzyme assay in which the product AMP is measured by coupling the PRPP synthetase reaction ($ATP + ribose\ 5 - phosphate \xrightarrow{2.7.6.1} PRPP + AMP$) to MK, PK, and LDH (Scheme 1) [56,57] in reaction mixtures containing 100 mM HEPES (pH 7.8), 25 mM MgCl$_2$, 2 mM ATP, 0.5 mM PEP, 300 μM NADH, 150 μM ribose-5-phosphate, 36 U mL^{-1} MK, 50 U mL^{-1} PK, and 36 U mL^{-1} LDH in a total volume of 250 μL. The ability of APRT2 to catalyze the reactions of adenosine phosphorylase (EC 2.4.2.1), and 5'-nucleotidase (EC 3.1.3.5) activities were also analyzed using the same methodology described for the discontinuous APRT activity assay (HPLC) above, with the following modifications. Samples (15 μL) were injected onto the column and eluted with a gradient from 5–40% Solvent B over 15.1 minutes at a flow rate of 0.425 mL min^{-1}. Solvent A: 20 mM ammonium acetate pH 4.5, Solvent B: 100% acetonitrile. Nucleobases and nucleosides were monitored at 260 nm. Assays to detect adenosine phosphorylase (EC 2.4.2.1) activity were carried out in Assay Buffer and contained 1 mM PRPP, 150 μM adenosine, 0.03 U inorganic pyrophosphatase (EC 3.6.1.1, Thermo Fisher Scientific) and APRT2 (25–50 μM). Assays to detect 5'-nucleotidase (EC 3.1.3.5) activity were carried out in Assay Buffer and contained 150 μM AMP, 4 μM *E. coli* K12 adenine deaminase (EC 3.5.4.2) [48], and APRT2 (25–50 μM). Assays were incubated for 30 min and overnight. Reactions were stopped by filtration to remove enzymes, using an Amicon Ultra (0.5 mL) filter with a 10,000 kDa cutoff, followed by centrifugation at 14,000 RPM for 25 min.

Cyanogen bromide cleavage of proteins

Cyanogen bromide cleavage reactions were performed as described in [58]. 10 μL of 5 M HCl were used to acidify 250 μg mL^{-1} of APRT2-Ntag, APRT2-Ctag, or APRT Ec (*E. coli* expressed

APRT2 stored in 5 mM DTT) in a total volume of 95 μL (Milli-Q water). 5 M Cyanogen bromide was added in 200 molar excess (200:1, CNBr/Met residue). APRT2 contains 5 Met residues, approximately 2.1% Met residue content. Samples were vortexed, covered with aluminum foil, and incubated for 24 hours at RT. The reaction was stopped by adding 5 volumes of Milli-Q water. Samples were dried using a vacufuge (60°C, 2 hours), resuspended in 50 μL water, and analyzed by 12% SDS-PAGE stained with Coomassie Blue.

Native mass spectrometry (MS)

APRT2-Ntag and APRT2-Ctag were buffer exchanged into a volatile buffer (200 mM ammonium acetate, pH 7.4) using a Micro Bio-Spin 6 device (Bio-Rad). Samples were loaded into pulled glass capillaries prepared in house, as described in [59], and introduced into an Orbitrap mass spectrometer (Exactive Plus with extended mass range (EMR), Thermo Scientific) by means of electro-spray ionization. The instrumental parameters were tuned to preserve the native-like structure of the proteins as described in [59].

Cloning, expression, and purification of wild-type and mutants of APRT2

APRT2 wild-type (WT), and mutants M73Q and M128Q, were codon optimized for expression in *E. coli* and cloned into pET-28a(+) vector, using *Nde*I and *Hind*III restriction sites (Genscript, USA). Optimal expression of all three proteins was obtained in BL21(DE3) cells, using Terrific-Broth media. The plasmids pET-28a(+)::*aprt2*, pET-28a(+)::*aprt2M73Q* and pET-28a(+)::*aprt2M128Q* were individually transformed into BL21(DE3) cells by heat-shock, and plates containing kanamycin 50 μg mL^{-1} were incubated overnight at 37°C. A single colony of each strain was used to inoculate 50 mL cultures of Terrific-Broth media in the presence of kanamycin 50 μg mL^{-1}. Starting cultures were incubated overnight at 37°C in an orbital shaker at 180 RPM. Starting culture (13mL) was used to inoculate 500 mL of Terrific-Broth media in the presence of kanamycin 50 μg mL^{-1}. Cultures were grown at 37°C and 180 RPM until the O.D.$_{600}$ reached 0.4–0.6. Protein expression was induced by the addition of IPTG to a final concentration of 1 mM. Cells were further grown under these conditions for 24 hours. Cells were harvested by centrifugation at 8,000 × g, washed with 50 mM Tris HCl (pH 7.4), 300 mM NaCl and stored at -20°C until purification. 5 grams of cell paste were resuspended in Resuspension Buffer and disrupted by sonication (15 cycles of 10 seconds at 60% amplitude) in the presence of 0.2 mg mL^{-1} lysozyme. After centrifugation at 48,000 × g, the N-terminal His-tagged protein was purified in a single step protocol using HisPur Ni-NTA resin (Thermo Fisher Scientific), equilibrated at RT. Protein binding was carried out in Resuspension Buffer supplemented with 20 mM imidazole. The bound protein was washed with increasing concentrations of imidazole (20–50 mM) in Resuspension Buffer and eluted in 10 CV of Resuspension Buffer containing 300–600 mM imidazole. Fractions containing apparently homogeneous APRT2 WT, APRT2 M73Q, and APRT2 M128Q, as inferred by SDS-PAGE (12% polyacrylamide; stained with Coomassie Blue), were pooled and dialyzed against 50 mM EPPS (pH 8.0), 300 mM NaCl. 5 mM DTT was added to APRT2 WT to ensure Met residues potentially oxidized during cell lysis were fully reduced. Homogeneous recombinant proteins were stored in presence of 10% (v/v) glycerol at -80°C.

APRT2 mutant M156Q was cloned, expressed, and purified as described above, with the following modifications: APRT2 M156Q best expression was observed in C43(DE3) cells, using Terrific-Broth media. After IPTG induction, cells were grown for 24 hours at 18°C. Homogeneous APRT2 M156Q, as inferred by 12% SDS-PAGE stained with Coomassie Blue, was pooled, dialyzed, and stored under the same conditions described above.

Data analysis

Data analysis was performed using GraphPad Prism 9.2 software. Initial velocity data obtained at variable concentrations of a single varied substrate *A* at fixed concentrations of another substrate were fitted to Eq (1), in which v is the initial velocity, E_t is the enzyme concentration, k_{cat} is the turnover number, *A* is the concentration of the variable substrate, and K_a is the apparent Michaelis constant.

$$\frac{v}{E_t} = \frac{k_{cat}A}{K_a + A}$$

(1)

Initial velocity data obtained at variable concentrations of a single substrate *A* at changing-concentrations of a second substrate *B* were fitted to Eq (2), in which K_{ia} and K_a are the respective dissociation and Michaelis constants of *A*, and K_b is the Michaelis constant of substrate *B*.

$$\frac{v}{E_t} = \frac{k_{cat}AB}{K_{ia}K_b + K_bA + K_aB + AB}$$

(2)

For inhibition studies in which double-reciprocal plots of inhibitor (*I*) *vs.* variable substrate (*A*) conformed to apparent competitive, noncompetitive, or uncompetitive inhibition, respectively, initial velocity data (*v*) were fitted to Eqs (3)–(5), for which E_t is the concentration of enzyme, k_{cat} and K_a are, respectively, the turnover number and the Michaelis constant for substrate A, and K_{is} and K_{ii} are respectively, the apparent slope and intercept inhibition constants.

$$\frac{v}{E_t} = \frac{k_{cat}A}{K_a\left(1 + \frac{I}{K_{is}}\right) + A}$$

(3)

$$\frac{v}{E_t} = \frac{k_{cat}A}{K_a\left(1 + \frac{I}{K_{is}}\right) + A\left(1 + \frac{I}{K_{ii}}\right)}$$

(4)

$$\frac{v}{E_t} = \frac{k_{cat}A}{K_a + A\left(1 + \frac{I}{K_{ii}}\right)}$$

(5)

Results and discussion

T. brucei brucei genome data includes two putative *aprt* genes (APRT1 –Tb927.7.1780, and APRT2 –Tb927.7.1790) located in tandem on chromosome 7. To ascertain the catalytic activity of the protein products of these two genes, both were cloned, expressed, and purified individually. Upon evaluation of *in vitro* activity, APRT1 was capable of catalyzing the forward and reverse reactions of APRT (Figs 1, S4, S5 and S6), while APRT2 catalysis of the forward APRT reaction is negligible (Table 1 and S4 Fig). From the steady-state kinetic analysis of the forward reactions catalyzed by APRT1 and APRT2 at apparent saturating fixed concentration of PRPP,

Table 1. Apparent kinetic parameters of APRT1 and APRT2.

Enzyme	Variable substrate	Fixed substrate	Apparent kinetic parameters[a]		
			K_M (μM)	k_{cat} (s^{-1})	k_{cat}/K_M (× 10^3 M^{-1} s^{-1})
APRT1	Adenine (1.5–150 μM)	PRPP (1 mM)	3.7 ± 0.5	1.74 ± 0.03	470 ± 64
APRT2	Adenine (50–500 μM)	PRPP (1 mM)	253 ± 4	0.003 ± 0.0002	0.012 ± 0.0008

[a]Initial velocity data were fit to Eq (1) to afford apparent kinetic parameters

we determined apparent k_{cat} and K_M values for adenine (Table 1). APRT2 displays a significantly lower k_{cat}/K_M value ($> 40{,}000$-fold decrease) when compared to APRT1 (Table 1). Although the reverse activity catalyzed by APRT1 was detected, the extent of the conversion of AMP into adenine is minor when compared to APRT1 forward activity (2.5% conversion in an assay containing 25 μM APRT1 at RT, with 30 minutes incubation—S5 Fig). This observation supports the assumption that the primary cellular role of APRT1 is scavenging 6-amino purine bases from hosts and their incorporation into nucleotides and nucleic acids via the purine salvage pathway. A greater preference for the forward reaction can be expected for obligatory purine auxotrophs.

Notably, catalysis of the APRT biosynthetic reaction by APRT2 is negligible when compared to APRT1. Endogenous adenine is present in human plasma at a concentration of approximately 9 nM [60], a value almost 30,000 lower than the APRT2 determined apparent K_M for adenine (Table 1), implying the APRT activity detected is not biologically relevant under normal metabolic conditions. Adenine concentration in human serum is tightly regulated, as higher adenine concentrations are related to numerous medical conditions [61–63]. Moreover, high concentrations of adenine are toxic to bloodstream stage and procyclic stage *T. brucei* ($IC_{50} \sim 300$ μM) [40], corroborating our findings that APRT2 is not a physiologically relevant APRT in *T. brucei*. Furthermore, the nearly 100-fold increase in apparent K_M of adenine for APRT2, when compared to APRT1, suggests adenine is not the natural substrate for APRT2 (Table 1).

APRT1 was further characterized in terms of its kinetic mechanism. The initial velocity data of PRPP *vs.* adenine when plotted in double-reciprocal form (S6 and S7 Fig) conformed to an intersecting pattern, which indicated that a sequential bi-substrate mechanism is operative for APRT1. Fitting of the data to Eq (2) afforded the kinetic parameters shown in Table 2. In kind, double-reciprocal plots for the initial velocity data of adenine *vs.* PRPP also conformed to an intersecting pattern, providing nearly identical kinetic parameters for both PRPP and adenine, when compared to the PRPP *vs.* adenine initial velocity data (S6 Fig). *Leishmania donovani*, also a unicellular parasitic protozoa purine auxotroph with complex life cycle encompassing insect and human hosts, has a single cytosolic APRT (*Ld*APRT). When compared to *Ld*APRT, APRT1 presents a similar K_M for adenine but displays a decreased catalytic efficiency (k_{cat}/K_M) for both substrates, with a nearly 30-fold decrease for adenine, and a 100-fold decrease for PRPP (Table 2). The significant difference in catalytic efficiencies may seem baffling, however previously reported apparent kinetics for APRT1 [46] are in the same range as the true initial velocity constants determined under our experimental conditions. More so, the 6-oxopurine phosphoribosyltransferases, HG(X)PRTs, from *T. brucei brucei* have been characterized for their apparent kinetic constants [38] and present catalytic efficiencies

Table 2. Initial velocity data for the biosynthetic reaction of APRT1 and other characterized parasitic protozoan APRTs.

Enzyme	Variable Substrate	Kinetic parameters[a]						
	(μM)	K_{PRPP} (μM)	$K_{i,PRPP}$ (μM)	k_{cat}/K_{PRPP} (x 10^3 $M^{-1}s^{-1}$)	K_{Ade} (μM)	k_{cat}/K_{Ade} (× 10^3 $M^{-1}s^{-1}$)	k_{cat} (s^{-1})
*Tbb*APRT1	Adenine (1.5–50)	77 ± 12	61 ± 13	8.1 ± 1.3	2.2 ± 0.7	282 ± 90	0.62 ± 0.02
	PRPP (10–250)	68 ± 11	22 ± 13	9.0 ± 1.6	2.3 ± 0.4	265 ± 49	0.61 ± 0.04
*Ld*APRT[b]	Adenine (2.5–50)	25 ± 6	N.D.	708 ± 282	2.3 ± 1.3	7782 ± 5027	17.9 ± 5.6
*Gl*APRT[c]	Adenine (3–10)	143 ± 47	376	19.6 ± 6.5	4.2 ± 0.6	595 ± 91	2.5 ± 0.14

[a]Initial velocity data were fit to Eq (2) to afford kinetic parameters.

[b]Data for *Leishmania donovani* APRT (*Ld*APRT) obtained by Bashor *et. al.*, 2002

[c]Data for *Giardia lamblia* APRT (GlAPRT) obtained by Sarver *et. al*, 2002

N.D. = not determined

Table 3. Dead-End inhibition data of 9-deazaadenine against varied adenine and PRPP.

9-deazaadenine	Variable Substrate	Fixed Substrate	Inhibition Pattern[a]	Apparent inhibition parameters[b]	
				K_{is} (μM)	K_{ii} (μM)
(0–300 μM)	Adenine (2.5–150 μM)	PRPP (1 mM)	C	156 ± 21	-
(0–600 μM)	PRPP (15–1000 μM)	Adenine (100 μM)	UC	-	404 ± 25

[a]C = Competitive inhibition, UC = Uncompetitive inhibition
[b]Initial velocity data for 9-deazaadenine *vs.* varied adenine fit best to Eq (3) and initial velocity data for 9-deazaadenine *vs.* varied PRPP fit best to Eq (5).

similar to the 6-amino phosphoribosyltransferase APRT1 (Table 2). It is our experience that the *T. brucei brucei* phosphoribosyltransferases are several fold less efficient than the closely related *Trypanosoma cruzi* homologues (manuscripts in preparation and [64]). While both *L. donovani* and *T. cruzi* are intracellular parasites, *T. brucei* infect host's extracellular fluids. One can speculate if this difference on their life cycles could have had an impact on the selective pressure for the evolution of enzymes with lower catalytic efficiency to reflect the concentration of free substrates available in the host's microenvironments. The concentration of adenine in human plasma, for example, is approximately 9 nM [60], whereas its intracellular concentration is estimated to be 1 μM [65]. Likewise, the extracellular protozoan parasite *Giardia lamblia* also contains a single APRT (*Gl*APRT), and when compared to APRT1 presents similar k_{cat}/K_M values for both PRPP and adenine.

The order of substrate binding and product release for APRT1 was determined by analysis of the dead-end inhibitor 9-deazaadenine (Table 3 and Figs 2 and S8), where 9-deazaadenine behaves as a competitive inhibitor to adenine as indicated by the double-reciprocal plots of initial velocity data at apparent saturating concentrations of PRPP, fixed-changed concentrations of 9-deazaadenine, and variable concentrations of adenine (Fig 2). At increasing fixed concentrations of 9-deazaadenine the intercept is not changed ($1/V_{max}$) but the slope (K_M/V_{max}) is changed, indicative of competitive inhibition and suggesting 9-deazaadenine and adenine bind to the same enzyme forms.

Double reciprocal plots of the initial velocity data at apparent saturating concentrations of adenine (100 μM) at fixed-changed concentrations of 9-deazaadenine *vs.* varying PRPP
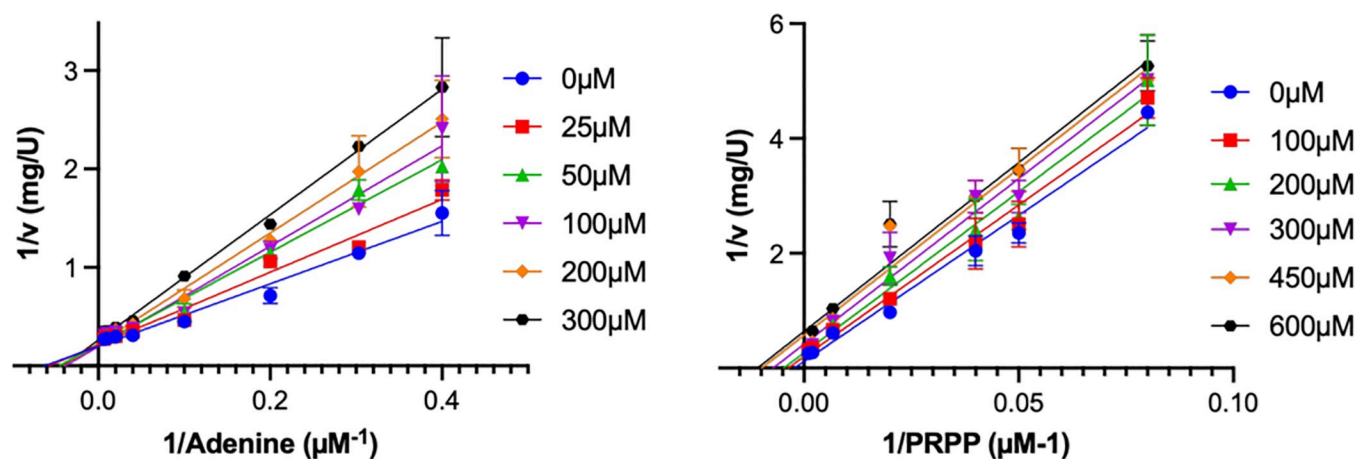

Fig 2. Double reciprocal plots of initial velocity data in the presence of the dead-end inhibitor 9-deazaadenine. (A) 9-deazaadenine is a competitive inhibitor *vs.* varied adenine (2.5–150 μM) at fixed apparent saturating concentrations of PRPP (1 mM) **(B)** 9-deazaadenine is an uncompetitive inhibitor *vs.* varied PRPP (12.5–1000 μM) at fixed apparent saturating concentrations of adenine (100 μM).
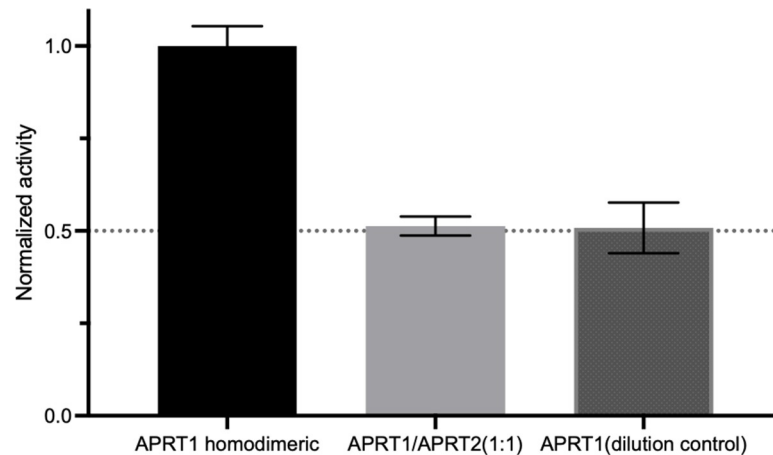
Fig 3. APRT activity as measured by AMP formation of reactions mixtures. Mixtures were composed of 150 μM adenine, 1 mM PRPP and 200 nM APRT1 (left), 200 nM APRT mixture (100 nM APRT1: 100 nM APRT2, middle), and 1:1 dilution of APRT1 in reaction buffer (100 nM APRT1, right).

https://doi.org/10.1371/journal.pntd.0009926.g003

provided an apparent uncompetitive pattern. At increasing concentrations of 9-deazaadenine the intercept is changed ($1/V_{max}$) but the slope (K_M/V_{max}) is unaffected, suggesting that PRPP binds to the enzyme before the addition of 9-deazaadenine. These results agree with the initial velocity data for APRT1 (Tables 1 and 2), and reveal a Bi-Bi sequential ordered kinetic mechanism, where the phosphoribosyl donor, PRPP, binds to free enzyme, followed by the second substrate, adenine. After catalysis, PP_i is the first product to dissociate from the enzyme-products complex, followed by the nucleoside monophosphate, AMP (S9 Fig). The possibility of a random mechanism is ruled out by these results, as in such case, a dead-end inhibitor mimic of the second substrate to bind the enzyme's active site, such as 9-deazaadenine, would behave as a mixed-type inhibitor to substrate PRPP [66]. Furthermore, sequential ordered mechanisms have been described and well conserved among the Type I phosphoribosyltransferases family of enzymes [67].

An ordered sequential mechanism has been previously described for *Ld*APRT [68]. The cytosolic *Ld*APRT [61–63] has higher sequence conservation to the cytosolic *T. brucei brucei* [40,46] APRT1 (52%) than to the glycosomal APRT2 (27%) [40,46]. Interestingly, *Gl*APRT was described to follow a unique reaction mechanism among phosphoribosyltransferases, in which there is a random addition of substrates (PRPP and adenine) followed by catalysis and an ordered release of the products, where PPi is the first product to leave the enzyme-products complex followed by AMP. *Gl*APRT primary sequence has 35% identity to APRT1 and 29% identity to APRT2.

APRT1 has been reported to adopt a dimeric quaternary structure (PDB code 5VN4), so we investigated whether a heterodimer of APRT1:APRT2 could form *in vitro* and provide a hybrid enzyme capable of catalysis. AMP formation was evaluated in reaction mixtures containing equimolar amounts of the two APRTs, which could give rise to three sets of dimers: APRT1 homodimers, APRT2 homodimers, and APRT1:APRT2 heterodimers in various ratios. AMP formation was reduced 2-fold from a control reaction mixture containing only APRT1 (Fig 3). The reduction in APRT activity is explained by the 1:1 dilution of APRT1, thereby indicating a catalytically active APRT1:APRT2 heterodimer is not formed. Such conclusion is supported by the activity observed when APRT1 is diluted in the reaction buffer to half of the control's concentration, as that would be the fraction of active enzyme present in the APRT1:APRT2 mixture if the enzymes do not interact and only APRT1 is catalytic active in the reaction mix.
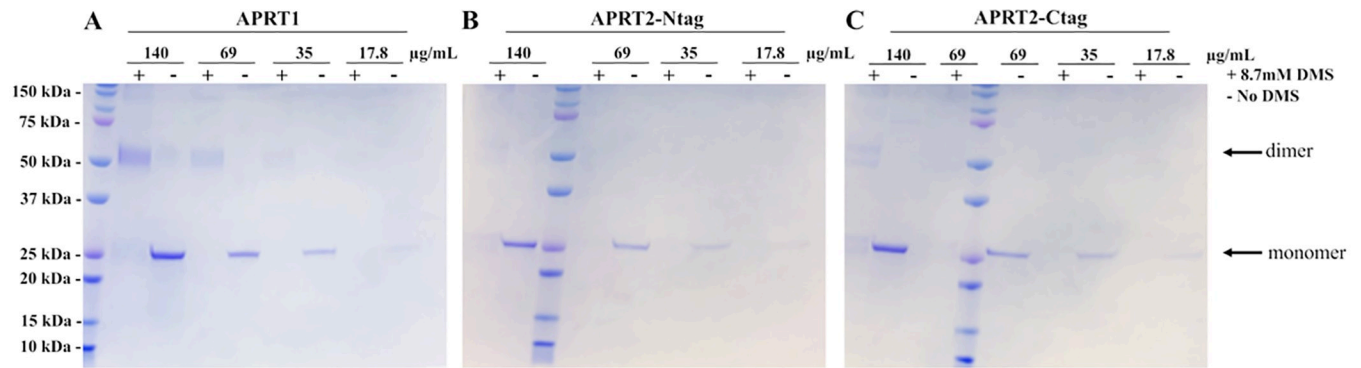
Fig 4. SDS-PAGE analysis of chemically crosslinked recombinant APRT1 and APRT2. APRT1 (**A**) homodimeric quaternary structure can be visualized under crosslinking assay conditions in concentrations ≥ 35 µg mL^{-1}, in presence of crosslink reagent DMS (8.7 mM), indicated by (+). Negative control lanes (-) show APRT1 monomers. APRT2 expressed with N-terminal (**B**) or C-terminal (**C**) tags.

A recent study revealed APRT1 and APRT2 do not interact *in vivo*, with APRT1 displaying homodimeric properties both *in vivo* and *in vitro* [46], in agreement to results showed in Fig 3. Co-expression and co-immunoprecipitation of tagged APRT1 and APRT2 in bloodstream forms of *T. brucei* revealed tagged APRT2 to only recover tagged APRT2, while tagged APRT1 interacts with tagged and endogenous APRT1 [46]. These results corroborate the previously described weak expression of APRT2 in the bloodstream life stage, being predominantly expressed in procyclic *T. brucei* forms and localized to the glycosome, while cytosolic APRT1 in equally expressed in both life stages [31,40]. Combined these results indicate the interaction of APRT1 and APRT2 is unlikely due to different expression patterns along *T. brucei* life cycle and their mismatched subcellular localization.

The quaternary structure of APRT1 and APRT2 was evaluated *in vitro* by treating APRT1 and APRT2 with DMS, an agent that chemically crosslinks two lysine residues within a mono-mer and also between lysine residues found in two or more associated monomers (Fig 4) [51]. Analysis of crosslinked proteins by denaturing polyacrylamide electrophoresis will show homodimers and other multimers, indicating quaternary structure, which will still be observed after significant protein dilution. Purified APRT1 (17.8–140 µg mL^{-1}) was treated with 8.7 mM DMS at pH 8.5. Our results corroborated the finding that APRT1 forms homodimers *in vitro*, as indicated by the observed dimeric structures, which is maintained after 4-fold dilution. To ensure the C-terminally localized glycosomal signal sequence of APRT2 did not obstruct dimerization events, APRT2 crosslinking assays were performed using recombinant enzyme expressed using pPICZ-Ntag (APRT2-Ntag) and pPICZ-Ctag (APRT2-Ctag) vectors (S2 Fig). There was no significant difference observed between APRT2-Ntag and APRT2-Ctag, and both show less frequent formation of a dimeric quaternary structure, which is not maintained after dilution as compared to APRT1 under identical concentrations and conditions (Fig 4). Size-exclusion chromatography (SEC) showed the recombinant APRT1 and APRT2 expressed in *P. pastoris* do not form aggregates in solution and corroborate the observed homodimeric quaternary structure of APRT1 (S10 Fig). Interestingly, SEC results for APRT2 indicate a dimeric quaternary structure, although the presence of two peaks with almost identical elution time may be an indicative of lower stability of such quaternary structure in solution when compared to APRT1 (S10 Fig), as observed in the crosslinking assay.

APRTs belong to the Type 1 phosphoribosyltransferases (Type 1 PRTases) family of homol-ogous enzymes and regulatory proteins of the nucleotide synthesis and salvage pathways. The alignment of APRT1 and APRT2 primary sequences using ClustalW [69] showed that only
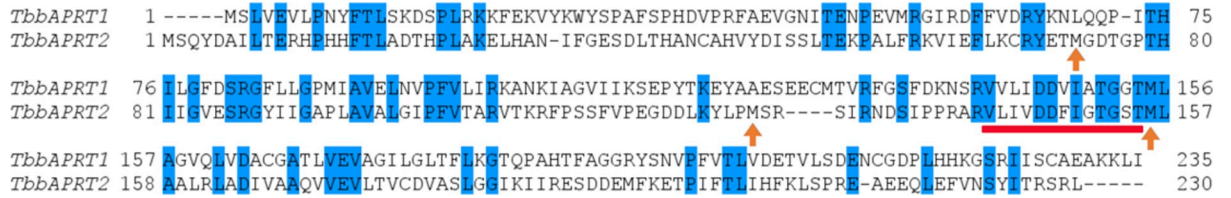
Fig 5. Alignment of *T. brucei brucei* APRT1 and APRT2. Conserved residues are shaded in blue. The conserved PRPP binding domain—a 13 residues-long active site loop—is underlined in red. APRT2 mutated methionine residues (M to Q) are indicated by orange arrows.

22% of their amino acids are conserved (Fig 5). Type 1 PRTases share highly conserved structures, but low levels of sequence identity except for the PRPP binding motif [67]. This motif is conserved in both APRT1 (VVLIDDVIATGGT), and APRT2 (VLIVDDFIGTGST) (Fig 5 - red underline and S11 Fig). A BLASTp search (https://blast.ncbi.nlm.nih.gov/Blast.cgi) using APRT2 as the query sequence classifies it as a Type 1 PRTase, with no other homology matches. The lack of relevant APRT activity suggests that APRT2 may play an alternative metabolic role. Low sequence identity does not preclude conservation of function for this family of proteins and since APRT2 presents the conserved PRPP binding motif, we tested the putative APRT2 activity as a Type 1 PRTase using other potential substrates. No phosphoribosyl transfer could be detected in the presence of hypoxanthine, guanine, xanthine, orotate, or uracil, ruling out possible HGXPRT (EC 2.4.2.8), OPRT (EC 2.4.2.10), or UPRT (EC 2.4.2.9) activities respectively (S12 Fig). Neither adenosine phosphorylase (EC 2.4.2.1), 5'-nucleotidase (EC 3.1.3.5), nor PRPP synthetase (EC 2.7.6.1) activities could be detected under our assay conditions (S12 and S13 Figs).

A recent publication showed that RNAi silencing of both APRT1 and APRT2 activity in *T. brucei* bloodstream stage cells did not produce a major growth phenotype, indicating the HGXPRT activity is adequate to maintain cell growth under normal growth conditions [46]. When the same RNAi cell line was tested as bloodstream stage cells grown in medium containing adenine as the sole available purine, a significant growth phenotype was observed suggesting the APRTs are the only enzymes that can incorporate adenine into the purine salvage pathway. The same publication reported another RNAi cell line, silencing APRT1 activity only, which displayed a growth phenotype similar to the bloodstream stage cells grown in medium containing only adenine, suggesting APRT2 is not able to compensate for the loss of APRT1 even when media contained up to 50 µM adenine [46].

What thus, can be the role or function of APRT2? The existing literature on APRT2 provides no data on its catalysis or metabolic role. Along with its localization to the glycosome and expression in the procyclic life stage [40,70], a co-immunoprecipitation study identified APRT2 as a protein associated with TbTim17, the major component of the mitochondrial inner membrane translocase complex in trypanosomes, with detection of a post-translational modification (PTM), in which a methionine residue of APRT2 was fully oxidized to methionine sulfoxide (MetO) [45]. PTMs have been described in trypanosomes [71] and are a freely reversible mechanism of control at the protein level that would enable the parasites to react quickly to environmental changes, including the presumably abrupt changes associated with vector (tsetse fly) to host transmission [72]. The metabolic change in procyclic trypanosomes from glycolysis to oxidative phosphorylation due to activation of the mitochondrion [73,74] could enable reactive oxygen species (ROS) to oxidize a Met residue to MetO [75]. The reversible formation of MetO by ROS as a mechanism of enzymatic activation has been described [76,77]; and the enzyme that mediates the reversal of this oxidation, methionine sulfoxide reductase, is putatively localized in the *T. brucei* genome (Tb927.8.550).

Utilizing a eukaryotic expression, such as *P. pastoris*, provided many advantages including occurrence of PTMs [78], and the oxidation of methionine residues have been previously reported in other heterologous proteins expressed in *P. pastoris* [79,80]. We employed the methionine-specific agent, cyanogen bromide (CNBr), to determine if (any) methionine residues in the APRT2 expressed in *P. pastoris* were oxidized into MetO. We utilized APRT2 expressed in *E. coli* (APRT2 Ec)—an expression system incapable of performing PTMs—as a negative control. APRT2 Ec was stored in the presence of the reducing agent DTT (5 mM) following purification to ensure methionine residues potentially oxidized during cell lysis were fully reduced. Peptide cleavage at the C-terminus of methionine residues in proteins by treatment with CNBr is a selective method to identify the presence of oxidized methionine residues in proteins as these will be refractory to this chemistry [81]. APRT2 has five methionine residues in its primary sequence. Treatment of recombinant APRT2 with 0.5 M HCl (final concentration) was followed by the addition of 250 mM CNBr. Analysis of the resulting protein fragments was observed utilizing SDS-PAGE. Recombinant APRT2 expressed in *P. pastoris* (APRT2-Ntag and APRT2-Ctag) provided identical patterns to the control (APRT2 Ec). Thereby indicating that both APRT2-Ntag and APRT2-Ctag, did not present a MetO PTM on any of the five known methionine residues present on its primary sequence (Fig 6A). Indeed, the resulting protein fragments provide bands with apparent molecular masses indicated on S14 Fig, where none of the 5 methionine residues are oxidized to MetO. These results were
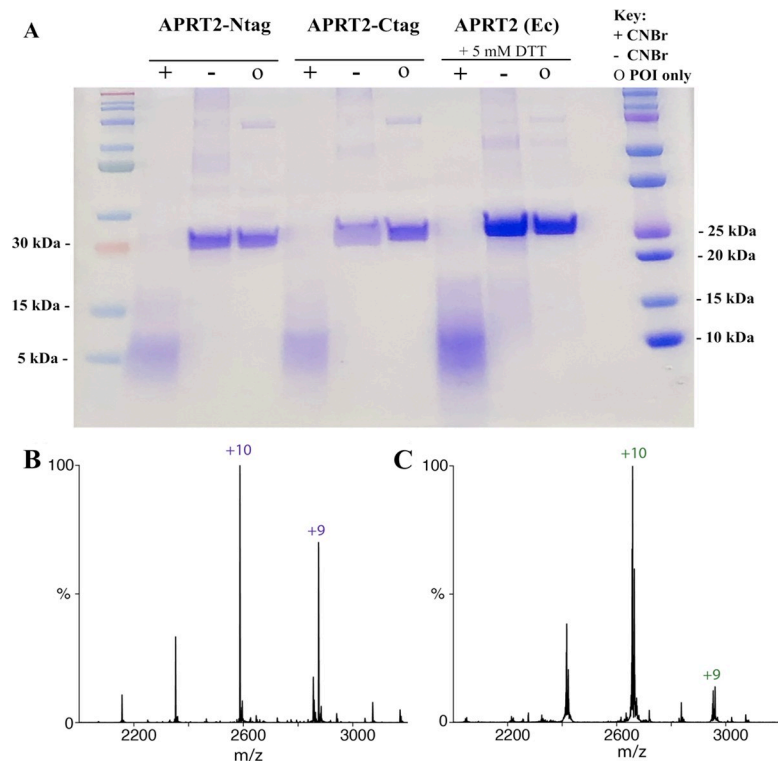

Fig 6. SDS-PAGE analysis of CNBr cleavage reaction (A) and Native-MS of recombinant APRT2s (B, C). (A) When APRT2 methionine residues are not oxidized to MetO, bands of molecular mass with the expected sizes indicated in S14 Fig would be observed. APRT2 expressed in *E. coli* and stored in the presence of 5 mM DTT (APRT2 Ec) was used as a control. The bands resulting from CNBr cleavage for the APRT2-Ntag, APRT2-Ctag, and APRT2 Ec are shown in the (+) lanes. Negative controls (-) and untreated native protein (o) show the band corresponding to the monomer mass. Native-MS of recombinant APRT2-Ntag **(B)** and APRT2-Ctag **(C)** provided the measured masses of 25,860 and 26,637 Da, respectively.

https://doi.org/10.1371/journal.pntd.0009926.g006

confirmed with Native-MS, where a change of 16 Da on the protein subunit mass–equivalent to a MetO PTM, could not be identified (Fig 6B and 6C). The native MS of recombinant APRT2-Ntag and APRT2-Ctag provided the measured masses of 25,860 and 26,637 Da, respectively. The theoretical monoisotopic mass of APRT2-Ntag and APRT2-Ctag are 25, 853 and 26,647 Da, respectively. The absence of a 16 Da increase from the theoretical monoisotopic mass of APRT2 monomers confirmed the lack of MetO formation. These results agreed with our analysis of the CNBr treatment, indicating that none of the recombinant APRT2s contained a MetO modification. Interestingly, the APRT2-Ntag also displayed a dimer with a mass of 51,739 Da, providing evidence that the C-terminal glycosomal signaling peptide may be involved in dimer formation. A dimeric oligomeric state was also detected using SEC (S10 Fig); however, crosslinking recombinant APRT2-Ntag with DMS did not provide evidence for a stable dimeric quaternary structure, as the dimeric multimer is not maintained after sufficient dilution under the tested conditions, indicating APRT2-Ntag dimers are likely unstable (Fig 4).

Due to the apparent absence of MetO formation in recombinant APRT2, we introduced methionine to glutamine (M to Q) mutations to mimic this PTM. The mutation of methionine residues to glutamine has previously been found to mimic the functional effects of a MetO, since both glutamine and MetO present an oxygen atom at the same position in their side chains and exhibit roughly the same hydrophobicity index value [75,82]. The crystallographic structure of APRT1 shows two methionine residues located near the PRPP binding site and one methionine residue located near the subunit interface, respectively M129, M155, and M89, numbered according to APRT1 primary sequence (S15 Fig). The APRT2 methionine residues located in the corresponding positions to APRT1 (M73, M128, and M156, according to APRT2 the primary sequence–Fig 5, orange arrows) were mutated to glutamine and the recombinant mutated proteins were analyzed for APRT activity. The forward reaction was monitored in presence of inorganic pyrophosphatase (EC 3.6.1.1) to displace the reaction equilibrium towards AMP formation: adenine + PRPP → AMP + PPi → 2P. APRT1 was used as a reaction control, and the complete conversion of adenine into AMP was observed in both control assay conditions (30 minute and overnight incubation). The three APRT2 M to Q mutants (M73Q, M128Q, and M156Q) displayed negligible APRT activity even when the assay was performed overnight in the presence of high concentrations of enzyme (25 µM) (Figs 7 and S16). These data suggested that the presence of a MetO does not increase nor elicit the catalytic APRT activity of APRT2, and the absence of APRT activity observed is indeed a reflection of a misannotation of Tb927.7.1790 as a putative APRT enzyme.

Conclusion

As a purine auxotroph, *Trypanosoma brucei ssp.* rely on purine phosphoribosyltransferases to salvage purines from their hosts for the synthesis of purine monophosphates. The APRT activity is important not only in adenine and adenosine metabolism, but also for its role in the activation of adenine-based pro-drugs [40,42,43]. All trypanosomes present two putative *aprt* genes in tandem; however, this characteristic is not observed on the other parasitic protozoa. APRT activity is unannotated or absent in *Plasmodium falciparum* [83], and *Toxoplasma gondii* [84]. Both *L. donovani* [85] and *G. lamblia* [86] present a single *aprt* gene, and both *Ld*APRT and *Gl*APRT share higher sequence conservation to *T. brucei brucei* APRT1 (52% and 35%) than to APRT2 (27% and 29%).

The trypanosomal APRT2 gene clusters apart from APRT1 on phylogenetic analyses and is more closely related to OPRTs than to other Type 1 PRTases [40]. However, we were unable to show enzymatic activity using orotate as substrate for the phosphoribosyl transfer, nor other
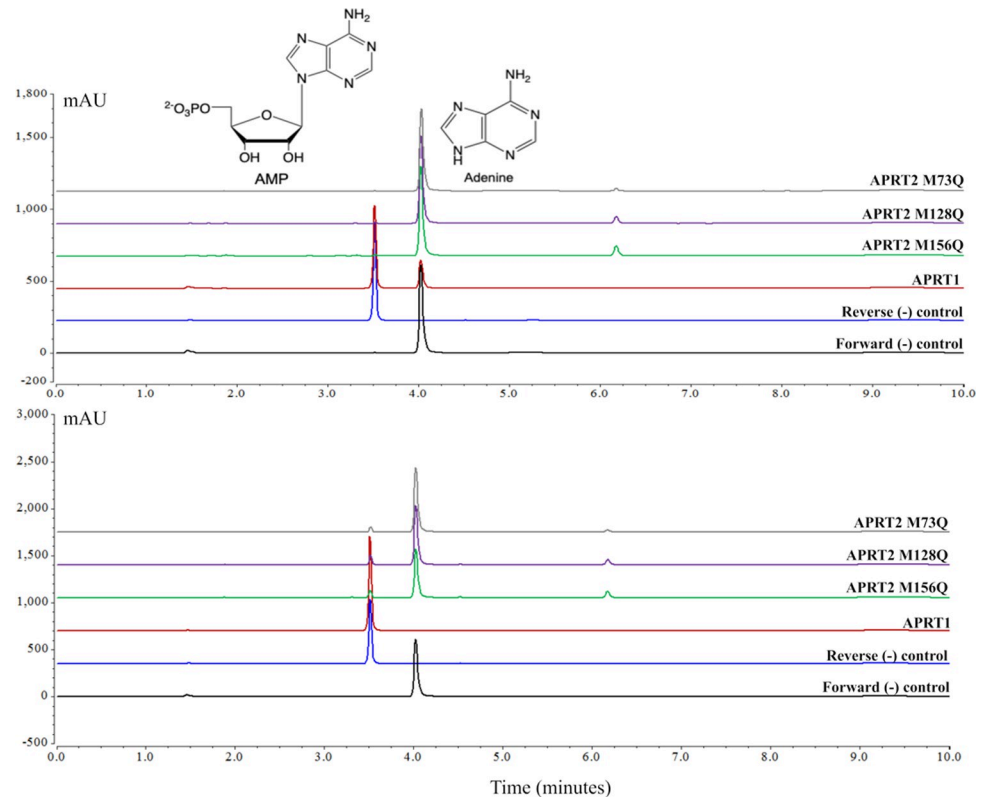
Fig 7. HPLC chromatograms of APRT2 M to Q mutants' activity. Activity assays of the APRT2 M to Q mutants' APRT activity assays with a 30 min (top graph) or overnight (bottom graph) incubation. Controls for the forward reaction showed the elution peak corresponding to adenine (Retention time (R_t) = 4.2 minutes, black lines), and reverse reaction showed the elution peak corresponding to AMP (R_t = 3.6 minutes, blue lines). The eluted peak at 6.2 minutes was present in all APRT2 assay fractions and could not be satisfactorily isolated and identified under current assay conditions.

https://doi.org/10.1371/journal.pntd.0009926.g007

purine bases known to be substrates of the Type 1 PRTases (S12 and S13 Figs). We could not detect any enzymatic activity when APRT2 was tested as a possible adenosine phosphorylase, 5'-nucleotidase, or PRPP synthetase (S12 and S13 Figs). The possibility of a PTM as a modulator of APRT activity was investigated, and APRT2 was shown to be unresponsive to MetO modifications as indicated by the lack of increased activity in the M to Q mutants (APRT2 M73Q, APRT2 M128Q, and APRT2 M156Q) (Figs 7 and S16). Some bacterial members of the Type 1 PRTases family seem to have no catalytic function, and instead act as expression regulators of genes involved in purine and pyrimidine synthesis [67]. Although a regulatory role for APRT2 cannot be ruled out at this moment, it is unlikely, as gene expression regulation in *Trypanosoma* is mainly achieved by post-transcriptional control [72], and the initiation of transcription by RNA polymerase II is not controlled for individual protein encoding genes [87]. A role of catalytic inactive enzymes, called prozymes, in activating their kinetically competent counterparts have been described in trypanosomes [88–90], where formation of hetero-oligomer complexes leads to activation or enhanced activity of the competent enzymes. The differential expression pattern of APRT1 and APRT2 [31,40], their localization in separate subcellular compartments [40, 46], results of co-expression and co-immunoprecipitation indicating absence of APRT1 and APRT2 interactions *in vivo* [46], and the *in vitro* assays presented here seem to indicate APRT2 is unlikely to act as a prozyme of APRT1. An example of gene duplication with loss of activity for the 6-aminophosphoribosyltransferases has been

described in *Saccharomyces cerevisiae*, were a second APRT, APRT2, was identified based on sequence identity, but later showed to be catalytically inactive based on *in vivo* complementation assays [91].

The characterization of APRT1 activity here and in a recently published study [46], its detection in proteomics [29,31], and higher sequence identity to other protozoan APRTs, allied to APRT2 lack of relevant catalytic APRT activity, indicate APRT1 is the only functional APRT enzyme in *T. brucei brucei*. Although APRT1 is located in the cytosol [40,46] while several other enzymes of the purine metabolism are glycosomal [28,31]; the subcellular localization of the purine salvage enzymes is not conserved among the protozoans, nor is this pathway restricted to a single subcellular compartment [40,92]. Our results reveal APRT1 has a greater preference for the forward reaction—in accordance with the parasite's nature as purine scavengers. *T. brucei* purine transporters show great affinity for the free purine bases [36,37], and the toxicity of high intracellular adenine concentrations is well described [40], highlighting the importance of phosphoribosyltransferases that greatly favor the forward reactions for incorporation of purine bases into nucleoside monophosphates. Our results provide a greater understanding of enzymes involved in adenine salvage, strengthening the ability to utilize APRT for therapeutic purposes in the development of drugs or pro-drugs of high selectivity and affinity. The role of APRT2, if any, in the purine salvage pathway, or as a Type 1 PRTase, requires further evaluation, while keeping in mind a possible event of gene duplication and loss of activity.

Supporting information

S1 Appendix. Optimized sequences of APRT1 and APRT2, showing the ORFs used for heterologous expression in *P. pastoris*, with N and C terminal overhangs used for cloning into pPICZ vectors (underlined).
(PDF)

S2 Appendix. Primers used for linearization of plasmids pET-28a(+)::*aprt1-Ntag*, pET-28a (+)::*aprt1-Ctag*, pET-28a(+)::*aprt2-Ntag* and pET-28a(+)::*aprt2-Ctag* prior to cloning into pPICZ vectors.
(PDF)

S1 Fig. Vector maps of APRT1-Ntag (left) and APRT1-Ctag (right). *P. pastoris* expression vector pPICZ maps, showing the *aprt1* gene insert position, and location of mCherry tags.
(PDF)

S2 Fig. Vector maps of APRT2-Ntag (left) and APRT2-Ctag (right). *P. pastoris* expression vector pPICZ maps, showing the *aprt2* gene insert position, and location of mCherry tags.
(PDF)

S3 Fig. Small scale expression screen of recombinant APRT1 and APRT2 in *P. pastoris*, co-expressed with mCherry. The highest expressing clones were selected based on mCherry expression levels (magenta color).
(PDF)

S4 Fig. Initial velocity data of APRT1 and APRT2 at apparent saturating concentrations of PRPP (1mM). The scale of the y-axis is significantly smaller for APRT2 when compared to APRT1
(PDF)

S5 Fig. HPLC chromatograms of APRT1 reverse activity. APRT reverse reaction was monitored in presence of adenine deaminase (EC 3.5.4.2) to favor adenine synthesis:

AMP + PPi → adenine + PRPP → hypoxanthine + NH_3. Forward reaction control shows the elution peak corresponding to adenine (R_t = 4.2 minutes, black line), and reverse reaction control shows the elution peak corresponding to AMP (R_t = 3.6 minutes, blue line). Although the reverse APRT activity is detected, the extent of the conversion of AMP (insert) into adenine is minor, under similar assay conditions, when compared to the forward reaction (Table 1).
(PDF)

S6 Fig. Bi-substrate kinetics of APRT1 forward reaction. (**A**) Initial velocities of APRT1 at fixed-changed PRPP concentrations, varying substrate adenine. (**B**) Initial velocities of APRT1 at fixed-changed adenine concentrations, varying substrate PRPP. Data Insets shows double reciprocal plots of A and B.
(PDF)

S7 Fig. Secondary reciprocal plots from initial velocity data with fixed and changed PRPP concentrations, varying substrate adenine. An apparent K_{ia} value was obtained with the secondary replot of the initial velocity double reciprocal slopes (right), shown in S6 Fig, where $slope = K_{ia}K_b/V_{max}$. Apparent K_{ia} was used as starting parameter for the global fitting of the initial velocity data using Eq (2), as described under Methods.
(PDF)

S8 Fig. Structure of adenine (left) and 9-deazaadenine (right).
(PDF)

S9 Fig. Ordered Bi Bi kinetic mechanism of APRT1 as obtained from initial velocity and dead-end inhibition studies.
(PDF)

S10 Fig. Size exclusion chromatography of APRT1 and APRT2. The elution volume of APRT1 (blue) and APRT2 (red) suggests both APRTs form homodimers and the SDS-PAGE analysis of eluted fractions illustrates the purity of the samples. The right upper figure shows the calibration curve (blue) for determining the oligomeric states of APRT1 (red) and APRT2 (green).
(PDF)

S11 Fig. Sequence alignment of APRT1, APRT2, and previously characterized APRTs. The amino acid residues conserved among all APRTs are highlighted in blue–reflecting the lower sequence conservation on the Type I phosphoribosyltransferases family of enzymes. The β-phosphoryl binding sequence is underlined in black; the catalytic loop sequence is underlined in green, and the PRPP binding domain is underlined in red. The C-terminal extension characteristic of the long APRTs is underlined in gray. The C-terminal glycosomal signaling peptide on *Tbb*APRT2 is boxed in orange. The conserved residue arginine 82 (*Tbb*APRT1 numbering–black dot) participates on binding of PRPP's β-phosphoryl group. Arginine 102 (gray dot) composes the active site of the adjacent subunit–highlighting the importance of the dimeric quaternary structure for catalytic activity. Tyrosine 121 (red dot) is located on the tip of the loop that closes over the active site after both substrates are bound, being essential for APRTs to adopt their catalytic conformation. For more details on the amino acid residues identified as essential for APRTs substrates binding and catalysis, refer [65,93,94].
(PDF)

S12 Fig. APRT2 Type 1 PRTase activity tests using alternative N-containing nucleophiles–part 1. APRT2 was tested for activity as a potential HGXPRT, EC 2.4.2.8 (**A**, **B**, **C**); OPRT, EC

2.4.2.10 (**D**), UPRT, EC 2.4.2.9 (**E**), and PRPP synthetase, EC 2.7.6.1 (**F**). No enzymatic activity could be detected under the assay conditions described in the Methods.
(PDF)

S13 Fig. APRT2 Type 1 PRTase activity tests using alternative N-containing nucleophiles– part 2. APRT2 was tested for activity as a potential adenosine phosphorylase, EC 2.4.2.1 (**A**), and 5'-nucleotidase, EC 3.1.3.5 (**B**). No enzymatic activity could be detected under the assay conditions described in the Methods.
(PDF)

S14 Fig. Expected fragments of APRT2 with no MetO modifications treated with cyanogen bromide. Cyanogen bromide selectively cleaves peptides at the C-terminus of reduced methionine residues. APRT2 contains five Met residues and when all Met residues are reduced, 6 fragments are produced. The molecular weight of all 6 fragments expected for APRT2-Ntag (**A**) and APRT2-Ctag (**B**) are depicted on each fragment.
(PDF)

S15 Fig. Location of methionine residues on APRT1 (PDB code 5VN4). The crystal structure of APRT1 shows 2 methionine residues located near the PRPP binding site (M129 and M155, upper right side) and one methionine residue located near the subunit interface (M85, lower right side). APRT1 subunits are colored in green and blue ribbons. Ligands (adenine and ribose-5-phosphate), as well as the methionine sidechains, are represented as sticks.
(PDF)

S16 Fig. HPLC chromatograms of APRT2 M to Q mutants' activity. APRT reverse reaction was monitored in presence of adenine deaminase (EC 3.5.4.2) to favor adenine synthesis: AMP + PPi $\rightarrow$ adenine + PRPP $\rightarrow$ hypoxanthine + NH_3. None of the three APRT2 M to Q mutants shows APRT reverse activity, either in 30 min (top graph) or overnight (bottom graph) incubations, as indicated by the invariable AMP peak and absence of formation of adenine. Forward reaction controls show the elution peak corresponding to adenine (black lines), and reverse reaction controls show the elution peak corresponding to AMP (blue lines). The eluted peak at 6.2 minutes was present in all APRT2 assay fractions (Fig 7) and could not be satisfactorily isolated and identified under current assay conditions.
(PDF)

Acknowledgments

Author Contributions

Conceptualization: Ardala Katzfuss.

Data curation: Ardala Katzfuss.

Formal analysis: Kayla Glockzin, Ardala Katzfuss.

Funding acquisition: Thomas D. Meek, Ardala Katzfuss.

Investigation: Kayla Glockzin, Ardala Katzfuss.

Methodology: Kayla Glockzin, Ardala Katzfuss.

Project administration: Ardala Katzfuss.

Supervision: Thomas D. Meek.

Validation: Kayla Glockzin, Ardala Katzfuss.

Writing – original draft: Kayla Glockzin, Ardala Katzfuss.

Writing – review & editing: Kayla Glockzin, Thomas D. Meek, Ardala Katzfuss.

References

1. Barrett MP, Burchmore RJ, Stich A, Lazzari JO, Frasch AC, Cazzulo JJ, et al. The trypanosomiases. Lancet. 2003; 362(9394):1469–80. Epub 2003/11/07. https://doi.org/10.1016/S0140-6736(03)14694-6 PMID: 14602444.

2. World Health Organization. Trypanosomiasis, human African (sleeping sickness) 2021.

3. Baker CH, Welburn SC. The Long Wait for a New Drug for Human African Trypanosomiasis. Trends Parasitol. 2018; 34(10):818–27. Epub 2018/09/06. https://doi.org/10.1016/j.pt.2018.08.006 PMID: 30181071.

4. Fenn K, Matthews KR. The cell biology of *Trypanosoma brucei* differentiation. Curr Opin Microbiol. 2007; 10(6):539–46. Epub 2007/11/13. https://doi.org/10.1016/j.mib.2007.09.014 PMID: 17997129; PubMed Central PMCID: PMC3902322.

5. Lindner AK, Priotto G. The unknown risk of vertical transmission in sleeping sickness—a literature review. PLoS Negl Trop Dis. 2010; 4(12):e783. Epub 2011/01/05. https://doi.org/10.1371/journal.pntd.0000783 PMID: 21200416; PubMed Central PMCID: PMC3006128.

6. Rocha G, Martins A, Gama G, Brandão F, Atouguia J. Possible cases of sexual and congenital transmission of sleeping sickness. The Lancet. 2004; 363(9404). https://doi.org/10.1016/S0140-6736(03)15345-7 PMID: 14738812

7. Lejon V, Bentivoglio M, Franco JR. Human African trypanosomiasis. Handb Clin Neurol. 2013; 114:169–81. Epub 2013/07/09. https://doi.org/10.1016/B978-0-444-53490-3.00011-X PMID: 23829907.

8. Kennedy PGE. Clinical features, diagnosis, and treatment of human African trypanosomiasis (sleeping sickness). The Lancet Neurology. 2013; 12(2):186–94. https://doi.org/10.1016/S1474-4422(12)70296-X PMID: 23260189

9. Berkowitz AL, Raibagkar P, Pritt BS, Mateen FJ. Neurologic manifestations of the neglected tropical diseases. J Neurol Sci. 2015; 349(1–2):20–32. Epub 2015/01/28. https://doi.org/10.1016/j.jns.2015.01.001 PMID: 25623803.

10. Langousis G, Hill KL. Motility and more: the flagellum of *Trypanosoma brucei*. Nat Rev Microbiol. 2014; 12(7):505–18. Epub 2014/06/17. https://doi.org/10.1038/nrmicro3274 PMID: 24931043; PubMed Central PMCID: PMC4278896.

11. Simarro PP, Jannin J, Cattand P. Eliminating human African trypanosomiasis: where do we stand and what comes next? PLoS Med. 2008; 5(2):e55. Epub 2008/02/29. https://doi.org/10.1371/journal.pmed.0050055 PMID: 18303943; PubMed Central PMCID: PMC2253612.

12. Neau P, Hanel H, Lameyre V, Strub-Wourgaft N, Kuykens L. Innovative Partnerships for the Elimination of Human African Trypanosomiasis and the Development of Fexinidazole. Trop Med Infect Dis. 2020; 5 (1). Epub 2020/02/06. https://doi.org/10.3390/tropicalmed5010017 PMID: 32012658; PubMed Central PMCID: PMC7157581.

13. Watson JA, Strub-Wourgaft N, Tarral A, Ribeiro I, Tarning J, White NJ. Pharmacokinetic-Pharmacodynamic Assessment of the Hepatic and Bone Marrow Toxicities of the New Trypanoside Fexinidazole. Antimicrob Agents Chemother. 2019; 63(4). Epub 2019/01/24. https://doi.org/10.1128/AAC.02515-18 PMID: 30670439; PubMed Central PMCID: PMC6496162.

14. Agency EM. CHMP recommends first oral-only treatment for sleepingsickness 2018. Available from: https://www.ema.europa.eu/en/news/chmp-recommends-first-oral-only-treatment-sleeping-sickness.

15. Mullard A. FDA approves first all-oral sleeping sickness drug. Nat Rev Drug Discov. 2021; 20(9):658. Epub 2021/08/08. https://doi.org/10.1038/d41573-021-00140-5 PMID: 34363026.

16. Deeks ED. Fexinidazole: First Global Approval. Drugs. 2019; 79(2):215–20. Epub 2019/01/13. https://doi.org/10.1007/s40265-019-1051-6 PMID: 30635838.

17. Hammarton TC. Cell cycle regulation in *Trypanosoma brucei*. Mol Biochem Parasitol. 2007; 153(1):1–8. Epub 2007/03/06. https://doi.org/10.1016/j.molbiopara.2007.01.017 PMID: 17335918; PubMed Central PMCID: PMC1914216.

18. Vassella E, Reuner B, Yutzy B, Boshart M. Differentiation of African trypanosomes is controlled by a density sensing mechanism which signals cell cycle arrest via the cAMP pathway. J Cell Sci. 1997; 110 (Pt 21):2661–71. Epub 1998/01/14. PMID: 9427384

19. Vanhollebeke B, Uzureau P, Monteyne D, Perez-Morga D, Pays E. Cellular and molecular remodeling of the endocytic pathway during differentiation of *Trypanosoma brucei* bloodstream forms. Eukaryot Cell. 2010; 9(8):1272–82. Epub 2010/06/29. https://doi.org/10.1128/EC.00076-10 PMID: 20581292; PubMed Central PMCID: PMC2918936.

20. Rotureau B, Van Den Abbeele J. Through the dark continent: African trypanosome development in the tsetse fly. Front Cell Infect Microbiol. 2013; 3:53. Epub 2013/09/26. https://doi.org/10.3389/fcimb.2013.00053 PMID: 24066283; PubMed Central PMCID: PMC3776139.

21. Schuster S, Kruger T, Subota I, Thusek S, Rotureau B, Beilhack A, et al. Developmental adaptations of trypanosome motility to the tsetse fly host environments unravel a multifaceted *in vivo* microswimmer system. Elife. 2017; 6. Epub 2017/08/16. https://doi.org/10.7554/eLife.27656 PMID: 28807106; PubMed Central PMCID: PMC5570225.

22. Cayla M, Rojas F, Silvester E, Venter F, Matthews KR. African trypanosomes. Parasit Vectors. 2019; 12(1):190. Epub 2019/05/01. https://doi.org/10.1186/s13071-019-3355-5 PMID: 31036044; PubMed Central PMCID: PMC6489224.

23. Kruger T, Schuster S, Engstler M. Beyond Blood: African Trypanosomes on the Move. Trends Parasitol. 2018; 34(12):1056–67. Epub 2018/09/06. https://doi.org/10.1016/j.pt.2018.08.002 PMID: 30181072.

24. Matovu E, Seebeck T, Enyaru JCK, Kaminsky R. Drug resistance in *Trypanosoma brucei* spp., the causative agents of sleeping sickness in man and nagana in cattle. Microbes and Infection. 2001; 3 (9):763–70. https://doi.org/10.1016/s1286-4579(01)01432-0 PMID: 11489425

25. Berriman M, Ghedin E, Hertz-Fowler C, Blandin G, Renauld H, Bartholomeu DC, et al. The genome of the African trypanosome *Trypanosoma brucei*. Science. 2005; 309(5733):416–22. Epub 2005/07/16. https://doi.org/10.1126/science.1112642 PMID: 16020726.

26. El-Sayed NM, Myler PJ, Bartholomeu DC, Nilsson D, Aggarwal G, Tran AN, et al. The genome sequence of *Trypanosoma cruzi*, etiologic agent of Chagas disease. Science. 2005; 309(5733):409–15. Epub 2005/07/16. https://doi.org/10.1126/science.1112631 PMID: 16020725.

27. El-Sayed NM, Myler PJ, Blandin G, Berriman M, Crabtree J, Aggarwal G, et al. Comparative genomics of trypanosomatid parasitic protozoa. Science. 2005; 309(5733):404–9. Epub 2005/07/16. https://doi.org/10.1126/science.1112181 PMID: 16020724.

28. Guther ML, Urbaniak MD, Tavendale A, Prescott A, Ferguson MA. High-confidence glycosome proteome for procyclic form *Trypanosoma brucei* by epitope-tag organelle enrichment and SILAC proteomics. J Proteome Res. 2014; 13(6):2796–806. Epub 2014/05/06. https://doi.org/10.1021/pr401209w PMID: 24792668; PubMed Central PMCID: PMC4052807.

29. Queiroz R, Benz C, Fellenberg K, Hoheisel JD, Clayton C. Transcriptome analysis of differentiating trypanosomes reveals the existence of multiple post-transcriptional regulons. BMC Genomics. 2009; 10:495. Epub 2009/10/28. https://doi.org/10.1186/1471-2164-10-495 PMID: 19857263; PubMed Central PMCID: PMC2772864.

30. Butter F, Bucerius F, Michel M, Cicova Z, Mann M, Janzen CJ. Comparative proteomics of two life cycle stages of stable isotope-labeled *Trypanosoma brucei* reveals novel components of the parasite's host adaptation machinery. Mol Cell Proteomics. 2013; 12(1):172–9. Epub 2012/10/24. https://doi.org/10.1074/mcp.M112.019224 PMID: 23090971; PubMed Central PMCID: PMC3536898.

31. Vertommen D, Van Roy J, Szikora JP, Rider MH, Michels PA, Opperdoes FR. Differential expression of glycosomal and mitochondrial proteins in the two major life-cycle stages of *Trypanosoma brucei*. Mol Biochem Parasitol. 2008; 158(2):189–201. Epub 2008/02/05. https://doi.org/10.1016/j.molbiopara.2007.12.008 PMID: 18242729.

32. de Azevedo WF Jr., Soares MB. Selection of targets for drug development against protozoan parasites. Curr Drug Targets. 2009; 10(3):193–201. Epub 2009/03/12. https://doi.org/10.2174/138945009787581186 PMID: 19275556.

33. Frankel MB, Knoll LJ. The ins and outs of nuclear trafficking: unusual aspects in apicomplexan parasites. DNA Cell Biol. 2009; 28(6):277–84. Epub 2009/04/08. https://doi.org/10.1089/dna.2009.0853 PMID: 19348590; PubMed Central PMCID: PMC2903460.

34. Campagnaro GD, Alzahrani KJ, Munday JC, De Koning HP. *Trypanosoma brucei* bloodstream forms express highly specific and separate transporters for adenine and hypoxanthine; evidence for a new protozoan purine transporter family? Mol Biochem Parasitol. 2018; 220:46–56. Epub 2018/01/27. https://doi.org/10.1016/j.molbiopara.2018.01.005 PMID: 29371154.

35. Landfear SM. Nutrient transport and pathogenesis in selected parasitic protozoa. Eukaryot Cell. 2011; 10(4):483–93. Epub 2011/01/11. https://doi.org/10.1128/EC.00287-10 PMID: 21216940; PubMed Central PMCID: PMC3127635.

36. de Koning HP, Jarvis SM. Adenosine transporters in bloodstream forms of *Trypanosoma brucei brucei*: substrate recognition motifs and affinity for trypanocidal drugs. Mol Pharmacol. 1999; 56(6):1162–70. Epub 1999/11/26. https://doi.org/10.1124/mol.56.6.1162 PMID: 10570043.

37. de Koning HP, Bridges DJ, Burchmore RJ. Purine and pyrimidine transport in pathogenic protozoa: from biology to therapy. FEMS Microbiol Rev. 2005; 29(5):987–1020. Epub 2005/07/26. https://doi.org/10.1016/j.femsre.2005.03.004 PMID: 16040150.

38. Dolezelova E, Teran D, Gahura O, Kotrbova Z, Prochazkova M, Keough D, et al. Evaluation of the *Trypanosoma brucei* 6-oxopurine salvage pathway as a potential target for drug discovery. PLoS Negl Trop Dis. 2018; 12(2):e0006301. Epub 2018/02/27. https://doi.org/10.1371/journal.pntd.0006301 PMID: 29481567; PubMed Central PMCID: PMC5843355.

39. Hammond DJ, Gutteridge WE. Purine and pyrimidine metabolism in the trypanosomatidae. Molecular and Biochemical Parasitology. 1984; 13(3):243–61. https://doi.org/10.1016/0166-6851(84)90117-8 PMID: 6396514

40. Luscher A, Lamprea-Burgunder E, Graf FE, de Koning HP, Maser P. *Trypanosoma brucei* adenine-phosphoribosyltransferases mediate adenine salvage and aminopurinol susceptibility but not adenine toxicity. Int J Parasitol Drugs Drug Resist. 2014; 4(1):55–63. Epub 2014/03/07. https://doi.org/10.1016/j.ijpddr.2013.12.001 PMID: 24596669; PubMed Central PMCID: PMC3940079.

41. Wallace LJ, Candlish D, Hagos A, Seley KL, de Koning HP. Selective transport of a new class of purine antimetabolites by the protozoan parasite *Trypanosoma brucei*. Nucleosides Nucleotides Nucleic Acids. 2004; 23(8–9):1441–4. Epub 2004/12/02. https://doi.org/10.1081/NCN-200027660 PMID: 15571273.

42. Parker WB, Allan PW, Waud WR, Hong JS, Sorscher EJ. Effect of expression of adenine phosphoribosyltransferase on the *in vivo* anti-tumor activity of prodrugs activated by *E. coli* purine nucleoside phosphorylase. Cancer Gene Ther. 2011; 18(6):390–8. Epub 2011/03/12. https://doi.org/10.1038/cgt.2011.4 PMID: 21394111; PubMed Central PMCID: PMC3096718.

43. Weckbecker G, Cory JG. 2,6-Diaminopurinedeoxyriboside as a prodrug of deoxyguanosine in L1210 cells. Cancer Res. 1987; 47(9):2218–23. Epub 1987/05/01. PMID: 3552212.

44. Fish WR, Looker DL, Joseph Marr J, Berens RL. Purine metabolism in the bloodstream forms of *Trypanosoma gambiense* and *Trypanosoma rhodesiense*. Biochimica et Biophysica Acta (BBA)—General Subjects. 1982; 719(2):223–31. https://doi.org/10.1016/0304-4165(82)90092-7 PMID: 6817814

45. Smith JT Jr., Singha UK, Misra S, Chaudhuri M. Divergent Small Tim Homologues Are Associated with TbTim17 and Critical for the Biogenesis of TbTim17 Protein Complexes in *Trypanosoma brucei*. mSphere. 2018; 3(3). Epub 2018/06/22. https://doi.org/10.1128/mSphere.00204-18 PMID: 29925672; PubMed Central PMCID: PMC6010621.

46. Dolezelova E, Klejch T, Spacek P, Slapnickova M, Guddat L, Hockova D, et al. Acyclic nucleoside phosphonates with adenine nucleobase inhibit *Trypanosoma brucei* adenine phosphoribosyltransferase in vitro. Sci Rep. 2021; 11(1):13317. Epub 2021/06/27. https://doi.org/10.1038/s41598-021-91747-6 PMID: 34172767; PubMed Central PMCID: PMC8233378.

47. Raran-Kurussi S, Cherry S, Zhang D, Waugh DS. Removal of Affinity Tags with TEV Protease. Methods Mol Biol. 2017; 1586:221–30. Epub 2017/05/05. https://doi.org/10.1007/978-1-4939-6887-9_14 PMID: 28470608; PubMed Central PMCID: PMC7974378.

48. Kamat SS, Bagaria A, Kumaran D, Holmes-Hampton GP, Fan H, Sali A, et al. Catalytic mechanism and three-dimensional structure of adenine deaminase. Biochemistry. 2011; 50(11):1917–27. Epub 2011/01/21. https://doi.org/10.1021/bi101788n PMID: 21247091; PubMed Central PMCID: PMC3059353.

49. Zheng R, Blanchard JS. Steady-state and pre-steady-state kinetic analysis of *Mycobacterium tuberculosis* pantothenate synthetase. Biochemistry. 2001; 40(43):12904–12. Epub 2001/10/24. https://doi.org/10.1021/bi011522+ PMID: 11669627.

50. Punekar NS. ENZYMES: Catalysis, Kinetics and Mechanisms 2018.

51. Davies GE, Stark GR. Use of dimethyl suberimidate, a cross-linking reagent, in studying the subunit structure of oligomeric proteins. Proc Natl Acad Sci U S A. 1970; 66(3):651–6. Epub 1970/07/01. https://doi.org/10.1073/pnas.66.3.651 PMID: 4913206; PubMed Central PMCID: PMC283100.

52. Breda A, Rosado LA, Lorenzini DM, Basso LA, Santos DS. Molecular, kinetic and thermodynamic characterization of *Mycobacterium tuberculosis* orotate phosphoribosyltransferase. Mol Biosyst. 2012; 8(2):572–86. Epub 2011/11/15. https://doi.org/10.1039/c1mb05402c PMID: 22075667.

53. Munagala N, Sarver AE, Wang CC. Converting the guanine phosphoribosyltransferase from *Giardia lamblia* to a hypoxanthine-guanine phosphoribosyltransferase. J Biol Chem. 2000; 275(47):37072–7. Epub 2000/09/08. https://doi.org/10.1074/jbc.M007239200 PMID: 10976110.

54. Keough D, Ng A-L, Winzor D, Emmerson B, de Jersey J. Purification and characterization of *Plasmodium falciparum* hypoxanthine–guanine–xanthine phosphoribosyltransferase and comparison with the human enzyme. Molecular and Biochemical Parasitology. 1999; 98(1):29–41. https://doi.org/10.1016/s0166-6851(98)00139-x PMID: 10029307

55. Villela AD, Ducati RG, Rosado LA, Bloch CJ, Prates MV, Goncalves DC, et al. Biochemical characterization of uracil phosphoribosyltransferase from *Mycobacterium tuberculosis*. PLoS One. 2013; 8(2): e56445. Epub 2013/02/21. https://doi.org/10.1371/journal.pone.0056445 PMID: 23424660; PubMed Central PMCID: PMC3570474.

56. Alderwick LJ, Lloyd GS, Lloyd AJ, Lovering AL, Eggeling L, Besra GS. Biochemical characterization of the *Mycobacterium tuberculosis* phosphoribosyl-1-pyrophosphate synthetase. Glycobiology. 2011; 21 (4):410–25. Epub 2010/11/04. https://doi.org/10.1093/glycob/cwq173 PMID: 21045009; PubMed Central PMCID: PMC3055594.

57. Donini S, Garavaglia S, Ferraris DM, Miggiano R, Mori S, Shibayama K, et al. Biochemical and structural investigations on phosphoribosylpyrophosphate synthetase from *Mycobacterium smegmatis*. PLoS One. 2017; 12(4):e0175815. Epub 2017/04/19. https://doi.org/10.1371/journal.pone.0175815 PMID: 28419153; PubMed Central PMCID: PMC5395218.

58. Andreev YA, Kozlov SA, Vassilevski AA, Grishin EV. Cyanogen bromide cleavage of proteins in salt and buffer solutions. Anal Biochem. 2010; 407(1):144–6. Epub 2010/07/31. https://doi.org/10.1016/j.ab.2010.07.023 PMID: 20670609.

59. Moghadamchargari Z, Huddleston J, Shirzadeh M, Zheng X, Clemmer DE, F MR, et al. Intrinsic GTPase Activity of K-RAS Monitored by Native Mass Spectrometry. Biochemistry. 2019; 58(31):3396–405. Epub 2019/07/16. https://doi.org/10.1021/acs.biochem.9b00532 PMID: 31306575; PubMed Central PMCID: PMC7196336.

60. Shi J, Liu H-F, Wong JM, Huang RN, Jones E, Carlson TJ. Development of a robust and sensitive LC–MS/MS method for the determination of adenine in plasma of different species and its application to *in vivo* studies. Journal of Pharmaceutical and Biomedical Analysis. 2011; 56(4):778–84. https://doi.org/10.1016/j.jpba.2011.07.023 PMID: 21840665

61. Slominska EM, Szolkiewicz M, Smolenski RT, Rutkowski B, Swierczynski J. High plasma adenine concentration in chronic renal failure and its relation to erythrocyte ATP. Nephron. 2002; 91(2):286–91. Epub 2002/06/08. https://doi.org/10.1159/000058406 PMID: 12053067.

62. Snyder FF, Hershfield MS, Seegmiller JE. Cytotoxic and metabolic effects of adenosine and adenine on human lymphoblasts. Cancer Res. 1978; 38(8):2357–62. Epub 1978/08/01. PMID: 667833.

63. Dos Santos IF, Sheriff S, Amlal S, Ahmed RPH, Thakar CV, Amlal H. Adenine acts in the kidney as a signaling factor and causes salt- and water-losing nephropathy: early mechanism of adenine-induced renal injury. Am J Physiol Renal Physiol. 2019; 316(4):F743–F57. Epub 2019/01/10. https://doi.org/10.1152/ajprenal.00142.2018 PMID: 30623725; PubMed Central PMCID: PMC6483032.

64. Wenck MA, Medrano FJ, Eakin AE, Craig SP. Steady-state kinetics of the hypoxanthine phosphoribosyltransferase from *Trypanosoma cruzi*. Biochim Biophys Acta. 2004; 1700(1):11–8. Epub 2004/06/24. https://doi.org/10.1016/j.bbapap.2004.03.009 PMID: 15210120.

65. Huyet J, Ozeir M, Burgevin MC, Pinson B, Chesney F, Remy JM, et al. Structural Insights into the Forward and Reverse Enzymatic Reactions in Human Adenine Phosphoribosyltransferase. Cell Chem Biol. 2018; 25(6):666–76 e4. Epub 2018/03/27. https://doi.org/10.1016/j.chembiol.2018.02.011 PMID: 29576532.

66. Segel IH. Enzyme Kinetics—Behavior and Analysis of Rapid Equilibrium and Steady-State Enzyme Systems. Hoboken, NJ, USA: Wiley Interscience Publication; 1993.

67. Sinha S. The PRT protein family. Current Opinion in Structural Biology. 2001; 11(6):733–9. https://doi.org/10.1016/s0959-440x(01)00274-3 PMID: 11751055

68. Bashor C, Denu JM, Brennan RG, Ullman B. Kinetic mechanism of adenine phosphoribosyltransferase from *Leishmania donovani*. Biochemistry. 2002; 41(12):4020–31. Epub 2002/03/20. https://doi.org/10.1021/bi0158730 PMID: 11900545.

69. Thompson JD, Higgins DG, Gibson TJ. CLUSTAL W: improving the sensitivity of progressive multiple sequence alignment through sequence weighting, position-specific gap penalties and weight matrix choice. Nucleic Acids Res. 1994; 22(22):4673–80. Epub 1994/11/11. https://doi.org/10.1093/nar/22.22.4673 PMID: 7984417; PubMed Central PMCID: PMC308517.

70. Dean S, Sunter JD, Wheeler RJ. TrypTag.org: A Trypanosome Genome-wide Protein Localisation Resource. Trends Parasitol. 2017; 33(2):80–2. Epub 2016/11/20. https://doi.org/10.1016/j.pt.2016.10.009 PMID: 27863903; PubMed Central PMCID: PMC5270239.

71. Torres-Gutierrez E, Perez-Cervera Y, Camoin L, Zenteno E, Aquino-Gil MO, Lefebvre T, et al. Identification of O-Glcnacylated Proteins in *Trypanosoma cruzi*. Front Endocrinol (Lausanne). 2019; 10:199.

Epub 2019/04/16. https://doi.org/10.3389/fendo.2019.00199 PMID: 30984116; PubMed Central PMCID: PMC6449728.

72. Clayton C, Shapira M. Post-transcriptional regulation of gene expression in trypanosomes and leishmanias. Mol Biochem Parasitol. 2007; 156(2):93–101. Epub 2007/09/04. https://doi.org/10.1016/j.molbiopara.2007.07.007 PMID: 17765983.

73. Dewar CE, MacGregor P, Cooper S, Gould MK, Matthews KR, Savill NJ, et al. Mitochondrial DNA is critical for longevity and metabolism of transmission stage *Trypanosoma brucei*. PLoS Pathog. 2018; 14 (7):e1007195. Epub 2018/07/19. https://doi.org/10.1371/journal.ppat.1007195 PMID: 30020996; PubMed Central PMCID: PMC6066258.

74. Prochazkova M, Panicucci B, Zikova A. Cultured bloodstream *Trypanosoma brucei* adapt to life without mitochondrial translation release factor 1. Sci Rep. 2018; 8(1):5135. Epub 2018/03/25. https://doi.org/10.1038/s41598-018-23472-6 PMID: 29572512; PubMed Central PMCID: PMC5865105.

75. Veredas FJ, Canton FR, Aledo JC. Methionine residues around phosphorylation sites are preferentially oxidized *in vivo* under stress conditions. Sci Rep. 2017; 7:40403. Epub 2017/01/13. https://doi.org/10.1038/srep40403 PMID: 28079140; PubMed Central PMCID: PMC5227694.

76. Drazic A, Winter J. The physiological role of reversible methionine oxidation. Biochim Biophys Acta. 2014; 1844(8):1367–82. Epub 2014/01/15. https://doi.org/10.1016/j.bbapap.2014.01.001 PMID: 24418392.

77. Kim G, Weiss SJ, Levine RL. Methionine oxidation and reduction in proteins. Biochim Biophys Acta. 2014; 1840(2):901–5. Epub 2013/05/08. https://doi.org/10.1016/j.bbagen.2013.04.038 PMID: 23648414; PubMed Central PMCID: PMC3766491.

78. Karbalaei M, Rezaee SA, Farsiani H. *Pichia pastoris*: A highly successful expression system for optimal synthesis of heterologous proteins. J Cell Physiol. 2020; 235(9):5867–81. Epub 2020/02/15. https://doi.org/10.1002/jcp.29583 PMID: 32057111; PubMed Central PMCID: PMC7228273.

79. Barral P, Tejera ML, Trevino MA, Batanero E, Villalba M, Bruix M, et al. Recombinant expression of Ole e 6, a Cys-enriched pollen allergen, in *Pichia pastoris* yeast: detection of partial oxidation of methionine by NMR. Protein Expr Purif. 2004; 37(2):336–43. Epub 2004/09/11. https://doi.org/10.1016/j.pep.2004.06.012 PMID: 15358355.

80. Shapiro RI, Wen D, Levesque M, Hronowski X, Gill A, Garber EA, et al. Expression of Sonic hedgehog-Fc fusion protein in *Pichia pastoris*. Identification and control of post-translational, chemical, and proteolytic modifications. Protein Expression and Purification. 2003; 29(2):272–83. https://doi.org/10.1016/s1046-5928(03)00062-7 PMID: 12767820

81. Parakra RD, Kleffmann T, Jameson GNL, Ledgerwood EC. The proportion of Met80-sulfoxide dictates peroxidase activity of human cytochrome c. Dalton Trans. 2018; 47(27):9128–35. Epub 2018/06/27. https://doi.org/10.1039/c8dt02185f PMID: 29944150.

82. McCarthy MR, Thompson AR, Nitu F, Moen RJ, Olenek MJ, Klein JC, et al. Impact of methionine oxidation on calmodulin structural dynamics. Biochem Biophys Res Commun. 2015; 456(2):567–72. Epub 2014/12/06. https://doi.org/10.1016/j.bbrc.2014.11.091 PMID: 25478640; PubMed Central PMCID: PMC4312012.

83. Mehrotra S, Bopanna MP, Bulusu V, Balaram H. Adenine metabolism in *Plasmodium falciparum*. Exp Parasitol. 2010; 125(2):147–51. Epub 2010/01/23. https://doi.org/10.1016/j.exppara.2010.01.002 PMID: 20093117.

84. Chaudhary K, Darling JA, Fohl LM, Sullivan WJ Jr., Donald RG, Pfefferkorn ER, et al. Purine salvage pathways in the apicomplexan parasite *Toxoplasma gondii*. J Biol Chem. 2004; 279(30):31221–7. Epub 2004/05/14. https://doi.org/10.1074/jbc.M404232200 PMID: 15140885.

85. Allen TE, Hwang H-Y, Jardim A, Olafson R, Ullman B. Cloning and expression of the hypoxanthine-guanine phosphoribosyltransferase from *Leishmania donovani*. Molecular and Biochemical Parasitology. 1995; 73(1–2):133–43. https://doi.org/10.1016/0166-6851(94)00105-v PMID: 8577321

86. Sarver AE, Wang CC. The adenine phosphoribosyltransferase from *Giardia lamblia* has a unique reaction mechanism and unusual substrate binding properties. J Biol Chem. 2002; 277(42):39973–80. Epub 2002/08/13. https://doi.org/10.1074/jbc.M205595200 PMID: 12171924.

87. Clayton C. Regulation of gene expression in trypanosomatids: living with polycistronic transcription. Open Biol. 2019; 9(6):190072. Epub 2019/06/06. https://doi.org/10.1098/rsob.190072 PMID: 31164043; PubMed Central PMCID: PMC6597758.

88. Volkov OA, Kinch L, Ariagno C, Deng X, Zhong S, Grishin N, et al. Relief of autoinhibition by conformational switch explains enzyme activation by a catalytically dead paralog. Elife. 2016; 5. Epub 2016/12/16. https://doi.org/10.7554/eLife.20198 PMID: 27977001; PubMed Central PMCID: PMC5201418.

89. Afanador GA, Tomchick DR, Phillips MA. Trypanosomatid Deoxyhypusine Synthase Activity Is Dependent on Shared Active-Site Complementation between Pseudoenzyme Paralogs. Structure. 2018; 26

(11):1499–512 e5. Epub 2018/09/11. https://doi.org/10.1016/j.str.2018.07.012 PMID: 30197036; PubMed Central PMCID: PMC6221947.

90. Hashimoto H, Kafkova L, Raczkowski A, Jordan KD, Read LK, Debler EW. Structural Basis of Protein Arginine Methyltransferase Activation by a Catalytically Dead Homolog (Prozyme). J Mol Biol. 2020; 432(2):410–26. Epub 2019/11/15. https://doi.org/10.1016/j.jmb.2019.11.002 PMID: 31726063; PubMed Central PMCID: PMC6995776.

91. Alfonzo JD, Crother TR, Guetsova ML, Daignan-Fornier B, Taylor MW. APT1, but not APT2, codes for a functional adenine phosphoribosyltransferase in *Saccharomyces cerevisiae*. J Bacteriol. 1999; 181 (1):347–52. Epub 1998/12/29. https://doi.org/10.1128/JB.181.1.347-352.1999 PubMed Central PMCID: PMC103569. PMID: 9864350

92. Zarella-Boitz JM, Rager N, Jardim A, Ullman B. Subcellular localization of adenine and xanthine phosphoribosyltransferases in *Leishmania donovani*. Mol Biochem Parasitol. 2004; 134(1):43–51. Epub 2004/01/30. https://doi.org/10.1016/j.molbiopara.2003.08.016 PMID: 14747142.

93. Shi W, Tanaka KS, Crother TR, Taylor MW, Almo SC, Schramm VL. Structural analysis of adenine phosphoribosyltransferase from Saccharomyces cerevisiae. Biochemistry. 2001; 40(36):10800–9. Epub 2001/09/06. https://doi.org/10.1021/bi010465h PMID: 11535055.

94. Ozeir M, Huyet J, Burgevin MC, Pinson B, Chesney F, Remy JM, et al. Structural basis for substrate selectivity and nucleophilic substitution mechanisms in human adenine phosphoribosyltransferase catalyzed reaction. J Biol Chem. 2019; 294(32):11980–91. Epub 2019/06/05. https://doi.org/10.1074/jbc.RA119.009087 PMID: 31160323; PubMed Central PMCID: PMC6690681.